

Root-to-shoot iron partitioning in *Arabidopsis* requires IRON-REGULATED TRANSPORTER1 (IRT1) protein but not its iron(II) transport function

Julia Quintana¹ , María Bernal^{1,2,*} , Marleen Scholle^{1,*} , Heike Holländer-Czytko¹, Nga T. Nguyen³ , Markus Piotrowski¹ , David G. Mendoza-Cózatl³ , Michael J. Haydon^{1,†}  and Ute Krämer^{1,*} 

¹Faculty of Biology and Biotechnology, Ruhr University Bochum, 44801 Bochum, Germany,

²Department of Plant Nutrition, Estación Experimental de Aula Dei-CSIC, 50059 Zaragoza, Spain, and

³Division of Plant Sciences, MU-Columbia, Columbia, MO 65211-7310, USA

Received 22 February 2021; revised 11 November 2021; accepted 15 November 2021; published online 28 November 2021.

*For correspondence (e-mail Ute.Kraemer@ruhr-uni-bochum.de).

†These authors contributed equally to this work.

†Present address: School of BioSciences, University of Melbourne, Parkville, VIC, 3010, Australia

SUMMARY

IRON-REGULATED TRANSPORTER1 (IRT1) is the root high-affinity ferrous iron (Fe) uptake system and indispensable for the completion of the life cycle of *Arabidopsis thaliana* without vigorous Fe supplementation. Here we provide evidence supporting a second role of IRT1 in root-to-shoot partitioning of Fe. We show that *irt1* mutants overaccumulate Fe in roots, most prominently in the cortex of the differentiation zone in *irt1-2*, compared to the wild type. Shoots of *irt1-2* are severely Fe-deficient according to Fe content and marker transcripts, as expected. We generated *irt1-2* lines producing IRT1 mutant variants carrying single amino-acid substitutions of key residues in transmembrane helices IV and V, Ser206 and His232, which are required for transport activity in yeast. Root short-term ⁵⁵Fe uptake rates were uninformative concerning IRT1-mediated transport. Overall *irt1*-like concentrations of the secondary substrate Mn suggested that the transgenic *Arabidopsis* lines also remain incapable of IRT1-mediated root Fe uptake. Yet, IRT1_{S206A} partially complements rosette dwarfing and leaf chlorosis of *irt1-2*, as well as root-to-shoot Fe partitioning and gene expression defects of *irt1-2*, all of which are fully complemented by wild-type IRT1. Taken together, these results suggest a regulatory function for IRT1 in root-to-shoot Fe partitioning that does not require Fe transport activity of IRT1. Among the genes of which transcript levels are partially dependent on IRT1, we identify *MYB DOMAIN PROTEIN10*, *MYB DOMAIN PROTEIN72* and *NICOTIANAMINE SYNTHASE4* as candidates for effecting IRT1-dependent Fe mobilization in roots. Understanding the biological functions of IRT1 will help to improve Fe nutrition and the nutritional quality of agricultural crops.

Keywords: Fe²⁺, homeostasis, iron deficiency, iron uptake, manganese, metal, MYB10, MYB72, NAS4, NRAMP1, nutrition, transceptor, ZIP.

Research highlights

- 1 Shoot Fe levels are very low in *Arabidopsis irt1* mutants lacking the well-known high-affinity root Fe²⁺ uptake system IRON-REGULATED TRANSPORTER1, but unexpectedly, *irt1* mutants overaccumulate Fe in roots.
- 2 A synthetic transport-inactive variant of IRT1, in which serine 206 is replaced by alanine, rescues the root-to-shoot Fe partitioning defect of *irt1*.
- 3 IRT1-dependent mobility of Fe from the root cortex to the shoot does not require IRT1-mediated Fe²⁺ transport, and *MYB10/MYB72* transcript levels are consistent with an involvement as downstream targets.

INTRODUCTION

The evolution of core components of electron transport chains and central metabolic pathways predated the Great Oxidation Event, which was accompanied by a dramatic decrease in the bioavailability of iron (Fe) approximately 2 billion years ago (Alberts et al., 2002). In all living organisms, the nutritional requirement for the micronutrient Fe is thus generally far higher than bioavailable concentrations in today's biosphere. Fe is the third most limiting mineral nutrient in agriculture (Zuo and Zhang, 2011), and one-third of the World's population suffer from Fe deficiency anemia (Lopez et al., 2016). As primary producers, land plants possess particularly effective mechanisms for mining Fe from the Earth's crust, and bioavailable Fe in plant biomass contributes to sustaining ecosystems and human nutrition.

IRON-REGULATED TRANSPORTER1 (IRT1) is the *bona fide* high-affinity root Fe²⁺ uptake system and of central importance in plants pursuing strategy I of Fe acquisition, including *Arabidopsis thaliana* (Connolly et al., 2002; Eide et al., 1996; Henriques et al., 2002; Kobayashi and Nishizawa, 2012; Varotto et al., 2002; Vert et al., 2002). *Arabidopsis irt1* mutants have severely chlorotic leaves, are strongly impaired in growth and die before reaching the reproductive stage unless supplemented with Fe chelates. The IRT1 protein forms a complex with FERRIC REDUCTION OXIDASE2 (FRO2) and AUTOINHIBITED PLASMA MEMBRANE H⁺-ATPase2 (AHA2) for Fe³⁺ solubilization and Fe²⁺ uptake into epidermal cells in the root differentiation zone (Martín-Barranco et al., 2020). Besides IRT1, the high-affinity Mn transporter NATURAL RESISTANCE-ASSOCIATED MACROPHAGE PROTEIN1 (NRAMP1) is thought to act as a secondary low-affinity Fe²⁺ uptake system (Cailliatte et al., 2010; Castaings et al., 2016).

In Fe-deficient plants, increased transcription of *IRT1*, *FRO2* and *AHA2* is controlled by the basic HELIX-LOOP-HELIX (bHLH) transcription factor FE DEFICIENCY-INDUCED TRANSCRIPTION FACTOR (FIT, bHLH29) (Bauer et al., 2007; Colangelo and Guerinot, 2004; Jakoby et al., 2004; Schwarz and Bauer, 2020). UPSTREAM REGULATOR OF IRT1 (URI)/bHLH121, in turn, mediates the transcriptional activation of *FIT* under Fe deficiency (Gao et al., 2020a; Kim et al., 2019; Gao et al., 2020b; Lei et al., 2020). Low Fe availability induces URI phosphorylation, which activates the formation of heterodimers of URI with bHLH34/104 or bHLH115 (ILR3) (Gao et al., 2020a; Kim et al., 2019). These heterodimers then bind to the promoters of several Fe deficiency-activated genes encoding regulators of Fe homeostasis in roots such as *MYB DOMAIN PROTEIN10* (*MYB10*)/*MYB DOMAIN PROTEIN72* (*MYB72*) and *bHLH38/39/100/101*. Notably, the interaction of transcription factors bHLH38/39/100/101 with FIT is necessary for the FIT-dependent activation of *IRT1*, *FRO2* and *AHA2*

(Sivitz et al., 2012; Wang et al., 2007). When a physiologically sufficient level of Fe is restored, FIT is polyubiquitinated by BRUTUS-LIKE1/2 (BTSL1/2) and targeted for degradation in the vacuole (Rodríguez-Celma et al., 2019; Sivitz et al., 2011).

IRT1 appears to undergo continuous cycling between the endosomal compartment and the plasma membrane where IRT1 is active (Barberon et al., 2011, 2014; Ivanov et al., 2014). The monoubiquitination of IRT1 triggers its trafficking from the plasma membrane to the early endosome, which can constitute the initial step towards the degradation of IRT1 in the vacuole (Barberon et al., 2011; Kerkeb et al., 2008). Monoubiquitination, internalization and degradation of IRT1 are strongly impaired in synthetic IRT1 variants carrying mutations of both lysine residues K154 and K179 in the cytosolic loop between transmembrane helices III and IV (Barberon et al., 2011; Kerkeb et al., 2008). SORTING NEXIN1 (SNX1) in the early endosome and the phosphatidylinositol-3-phosphate-binding protein FYVE-DOMAIN PROTEIN1 (FYVE1) in the late endosome contribute to the cellular sorting of IRT1, including its delivery to the plasma membrane that counteracts the degradation of endocytosed IRT1 protein (Barberon et al., 2014; Ivanov et al., 2014).

IRT1 lacks specificity for its primary substrate Fe²⁺ so that it can inadvertently transport other cations present in the soil solution, such as Mn²⁺, Cd²⁺, Zn²⁺ and Co²⁺ (Connolly et al., 2002; Eide et al., 1996; Rogers et al., 2000; Vert et al., 2002). For example, IRT1 was concluded to be the major route for the intake of non-essential hazardous Cd²⁺ cations into *Arabidopsis* and likely also into many food crops (Vert et al., 2002). To counteract the accumulation of toxic metals under Fe deficiency, excessive cytosolic levels of secondary-substrate metal cations are sensed by binding to a histidine-rich sequence motif in the cytosolic loop located between transmembrane helices III and IV of IRT1 (Dubeaux et al., 2018). This leads to the phosphorylation of serine and threonine residues in the same cytosolic loop of IRT1 by CBL-INTERACTING PROTEIN KINASE23 (CIPK23), thus triggering the extension of monoubiquitination into K63-polyubiquitination mediated by IRT1 DEGRADATION FACTOR1 (IDF1), followed by the vacuolar degradation of IRT1 (Dubeaux et al., 2018; Shin et al., 2013). FRO2 and AHA2 can also be ubiquitinated, but – different from IRT1 – their post-translational modification is independent of non-target secondary IRT1 substrate metal cations (Martín-Barranco et al., 2020).

Besides its localization at the root surface for Fe²⁺ cation uptake by the plant, IRT1 was also detected in the root vasculature (Barberon et al., 2011; Marquès-Bueno et al., 2016). Only the combined expression of *IRT1* in both root trichoblasts and phloem companion cells complemented the dwarfed growth, leaf chlorosis and infertility

of the *irt1* mutant cultivated in soil (Marquès-Bueno et al., 2016). Moreover, the *IRT1* mRNA was reported to move from the shoot into the root, suggesting its cell-to-cell mobility (Thieme et al., 2015). The function of *IRT1* expression in phloem companion cells has remained elusive to date.

Here we provide evidence for a secondary role of *IRT1* in root-to-shoot Fe partitioning, independent of its transmembrane Fe^{2+} transport activity. Our results show an overaccumulation of Fe in roots of the *irt1* mutant, whereas *irt1* shoots are severely Fe-deficient in comparison to wild-type (WT) plants. We transformed the *irt1* mutant with *IRT1* constructs encoding the transport-inactive mutant protein variants *IRT1*_{S206A} and *IRT1*_{H232A}. In these lines, short-term root Fe uptake rates and accumulation of the secondary *IRT1* substrate Mn are indistinguishable from those in *irt1*, as expected. Nevertheless, *IRT1*_{S206A} partially rescues rosette dwarfing and leaf chlorosis, as well as alterations in root-to-shoot Fe mobilization and Fe status marker transcript levels, of *irt1*. Using transcriptomics, we further identify *MYB10*, *MYB72* and their target of transcriptional activation *NICOTIANAMINE SYNTHASE4* (*NAS4*) as candidates for downstream involvement in *IRT1*-dependent root-to-shoot Fe partitioning, among other genes.

RESULTS

Root-to-shoot Fe partitioning is altered in the *irt1* mutant

To examine how Fe concentrations are altered in roots and shoots of the *irt1* mutant, we compared WT and *irt1-2* seedlings (*pam42*, termed *irt1* below). Seedlings were cultivated under Fe-deficient (–Fe, no added Fe) and Fe-sufficient (+Fe, 10 μM FeHBED, control) conditions for 10 days, subsequent to a 10-day pre-cultivation period on Fe-sufficient standard medium (Figure 1(a)). Upon cultivation in control conditions, shoot Fe concentrations were about one-third lower in *irt1* seedlings than in the WT (Figure 1(b)). On Fe-deficient media, Fe concentrations were equivalent in shoots of *irt1* and WT (Figure 1(b), Figure S1(a,b)). We attribute this to growth limitation by Fe deficiency, a general concept brought up earlier (Baxter et al., 2008). In roots, Fe concentrations were about twice as high in *irt1* than in the WT when cultivated under control conditions (Figure 1(c)). A similar trend was observed upon cultivation in Fe-deficient media, but the difference between *irt1* and WT was not statistically significant (Figure 1(c)). Thus, shoot Fe concentrations were in agreement with expectations, but root Fe concentrations were contrary to expectations, based on the role of *IRT1* as the

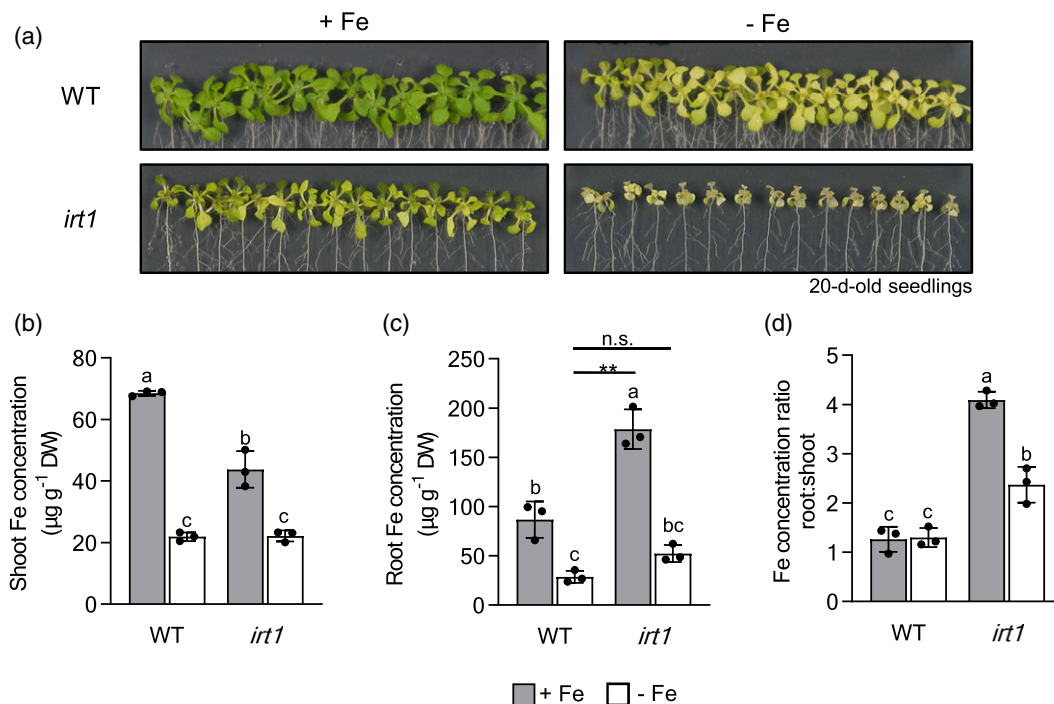


Figure 1. The *irt1* mutant overaccumulates Fe in the root whereas the shoot is Fe-limited.

(a) Photographs of 20-day-old WT and *irt1* seedlings grown in Fe-sufficient (+Fe, 10 μM FeHBED) and Fe-deficient (–Fe, 0 μM FeHBED) agar-solidified 0.25 \times modified Hoagland's medium (EDTA-washed agar) for 10 days, subsequent to an initial cultivation in standard medium (5 μM FeHBED, unwashed agar) for 10 days, on vertically oriented Petri plates. (b–d) Shoot (b) and root (c) Fe concentrations and root:shoot Fe concentration ratio (d) in 20-day-old WT and *irt1* seedlings. Seedlings were grown as in (a). Bars represent arithmetic mean \pm SD ($n = 3$ pools of tissue, each from 15 [WT] or 30 [*irt1*] seedlings, with 15 seedlings cultivated per plate/pool). Distinct letters indicate statistically significant differences ($P < 0.05$, two-way ANOVA followed by Tukey's HSD test). Data show one experiment representative of three independent experiments. DW: dry biomass.

primary root Fe uptake system of Arabidopsis. Congruent with these observations, root-to-shoot Fe concentration ratios were invariably close to unity in WT, but they were strongly shifted towards root Fe accumulation in *irt1* on both control and Fe-deficient media (Figure 1(d)). Accounting for condition- and genotype-dependent differences in the degree of Fe limitation of growth (Figure S1(a,b)), total Fe contents (Figure S1(c,d)) were also in agreement. We confirmed these observations also in the *irt1-1* mutant (WS genetic background, Figure S2). Taken together, our results suggest a substantial reduction in the partitioning of Fe from roots to shoots in *irt1* mutant plants, in addition to their previously described well-known Fe uptake defect (Henriques et al., 2002; Vert et al., 2002).

In order to address where overaccumulation of Fe occurs in the roots of *irt1* seedlings, we performed histochemical detection of non-heme Fe²⁺ or Fe³⁺ in roots after desorbing apoplastically bound Fe. We confirmed that roots of the constitutively Fe-deficient *frd3-7* mutant overaccumulate Fe in the stele, as previously reported (Green and Rogers, 2004). Whole-mount Perls staining of roots of seedlings grown on standard media was in agreement with elevated Fe levels in *irt1* compared to the WT, in which we did not observe any insoluble precipitates of Prussian blue (Figure 2). In *irt1* roots, the Perls stain was localized in the two sub-epidermal cell layers of the differentiation zone,

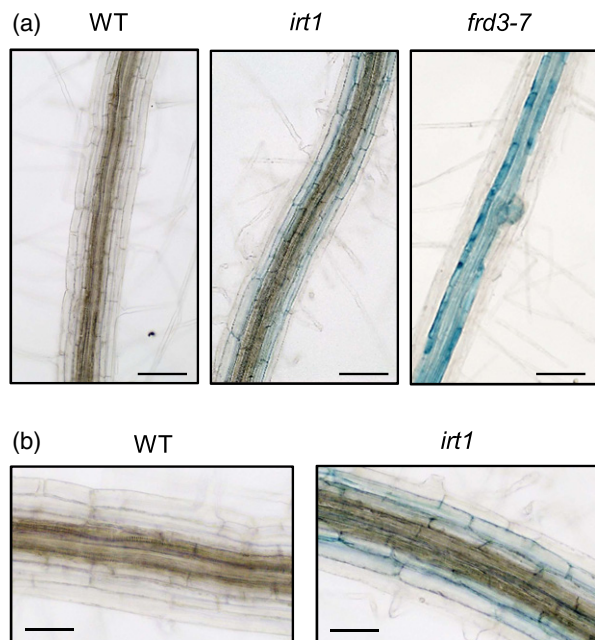


Figure 2. Fe accumulates in sub-epidermal cell layers of *irt1* roots. (a) Histochemical detection of labile Fe by Perls stain in the root differentiation zone of 7-day-old WT, *irt1* and *frd3-7* seedlings grown on agar-solidified 0.25× modified Hoagland's medium (5 μM FeHED). (b) Magnified image (20×) of WT and *irt1* roots shown in (a). Photographs are representative of $n = 10$ to 12 roots from two independent experiments, each with seedlings cultivated on three replicate Petri plates processed in parallel. Scale bars: 100 μm (a), 50 μm (b).

most prominently in the cortex, and not visible in the stele, different from the *frd3-7* mutant. This observation is consistent with impaired Fe movement into the stele of *irt1*, and it cannot be explained by the loss of the cellular Fe import function of IRT1, which is primarily localized in root epidermal cells (Marquès-Bueno et al., 2016; Vert et al., 2002).

IRT1_{S206A} variant partially complements the Arabidopsis *irt1* mutant

AtIRT1 unequivocally functions in plant Fe uptake by transporting Fe²⁺ cations across the plasma membrane of root epidermal cells (Vert et al., 2002). To test for any additional, distinct role of IRT1 in Fe homeostasis, we used site-directed mutagenesis for constructing variants of IRT1 (Figure S3) that encode IRT1_{S206A} (serine at position 206 substituted by alanine) and IRT1_{H232A} (histidine at position 232 substituted by alanine). Previous work had shown that both of these IRT1 mutant variants are unable to transport both Fe²⁺ and non-target substrates Zn²⁺, Mn²⁺ and Cd²⁺ in the heterologous yeast system *Saccharomyces cerevisiae* (Rogers et al., 2000). Genomic sequences corresponding to the coding region of IRT1 variants and WT IRT1 were placed downstream of the native IRT1 promoter (1024 bp) and upstream of the native genomic IRT1 terminator (310 bp). We obtained Arabidopsis *irt1* IRT1_{P::IRT1_{S206A} (termed *irt1* S206A) and *irt1* IRT1_{P::IRT1_{H232A} (*irt1* H232A) lines capable of producing transport-inactive IRT1 only, as well as complemented lines *irt1* IRT1_{P::IRT1} (*irt1* IRT1; Table S1). IRT1 transcripts were at comparable levels in the WT and the two complemented lines, and undetectable in the *irt1* mutant (Figure S4(a)). For both *irt1* S206A and *irt1* H232A, IRT1 transcript levels were comparable to the WT in one line and approximately tripled those of the WT in the other line, in -Fe-grown seedlings. By comparison, in +Fe-grown seedlings of WT and all transformant lines, IRT1 transcript levels were down to a small fraction of between 5 and 16%, except in the *irt1* H232A lines in which transcript levels in +Fe remained at between 64 and 89%, of those grown in -Fe. Note that in our transgenic *irt1* lines, IRT1 transcript levels are influenced by both the genomic environment of the transfer DNA (T-DNA) and the physiological Fe status of seedlings, some of which possess only a transport-inactive IRT1 protein. In contrast to IRT1, maximal IRT2 transcript levels remained below WT levels in all the different transformant lines. Thus, it appears that the T-DNA insertion in *irt1-2* (*pam42*), positioned within the transcribed region 96 bp upstream of the translational start codon of IRT1 and about 2700 bp downstream of the last exon of IRT2, also disrupted the function of IRT2 (Varotto et al., 2002).}}

IRT1 protein abundance in roots largely reflected IRT1 transcript levels (Figure 3(a), see Figure S4(a)). IRT1 protein levels were comparable to the WT in *irt1* S206A line 2 and elevated compared to both the complemented lines and the WT in line 1 (Figure 3(a), Figure S4(b)).

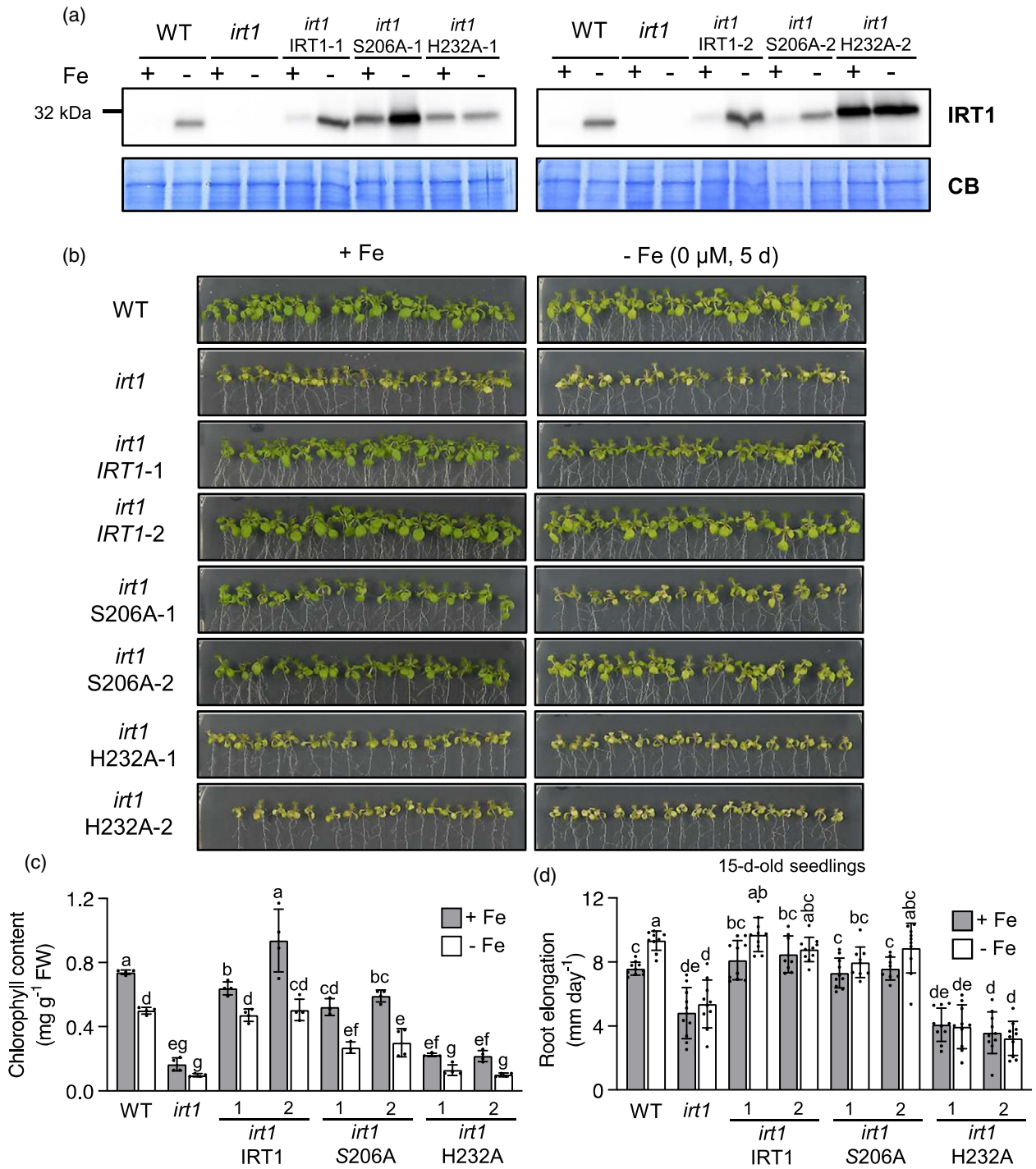


Figure 3. Fe transport-inactive IRT1^{S206A} partially complements *irt1*.

(a–d) Immunoblot detection of IRT1 protein (a), photographs (b), leaf chlorophyll concentrations (c) and mean root elongation over the last 5 days of growth (d) in 15-day-old seedlings of WT, *irt1*, *irt1* IRT1, *irt1* S206A and *irt1* H232A. Seedlings were grown on Fe-sufficient (+Fe, 10 μM FeHBED) and Fe-deficient (–Fe, 0 μM FeHBED) agar-solidified 0.25× modified Hoagland’s medium (EDTA-washed agar) for 5 days, subsequent to an initial cultivation period of 10 days in standard medium (5 μM Fe-HBED; unwashed agar), on vertically oriented Petri plates. Total root protein extracts (20 μg) were separated on denaturing gels and blotted onto PVDF membranes, with the Coomassie Blue-stained (CB) PVDF membrane shown as loading control (a). Bars represent arithmetic mean ± SD (*n* = 4 pools of 5 to 8 shoots (c); *n* = 8 to 10 roots (d)). Distinct letters indicate significant differences (*P* < 0.05) according to two-sample Student’s or Welch *t*-tests upon correction for multiple comparisons (c) or two-way ANOVA followed by Tukey’s HSD test (d). Images in (a) are representative of three replicate membranes. Data are from two independent experiments, each with two (c) or one (d) replicate plates per condition and genotype.

Importantly, IRT1 protein was detectable in roots of WT seedlings cultivated on our Fe-sufficient control media, supporting a role of IRT1 in Fe acquisition also under these cultivation conditions (Figure S4(b)).

In the two *irt1* S206A lines, seedling growth, rosette color, leaf chlorophyll concentrations and root growth all suggested a partial complementation of *irt1* mutant phenotypes by comparison to the WT and *irt1* IRT1 complemented lines (Figure 3(b–d)). By contrast, the *irt1* H232A lines resembled the *irt1* mutant throughout. Similarly, soil-grown vegetative *irt1* S206A plants were of a similar size and green color as the WT and *irt1* IRT1 complemented lines, whereas *irt1* H232A lines were indistinguishable from the *irt1* mutant (Figure S5). Rosettes of *irt1* S206A line 2 appeared to be slightly larger and greener than those of line 1 (Figure 3(b), Figure S5). The partial complementation of the *irt1* mutant phenotype through the IRT1_{S206A} variant of the *irt1* mutant phenotype through the IRT1_{S206A} variant of an amino acid residue required for transport activity is in agreement with our hypothesis of a secondary biological function of IRT1 in addition to transmembrane Fe²⁺ transport. The IRT1_{H232A} variant of IRT1 was unable to complement the *irt1* mutant phenotype, consistent with a model in which H232 is indispensable for both Fe transport and any additional role in Fe homeostasis carried out by IRT1.

Next we sought to confirm that the *irt1* S206A and *irt1* H232A mutants cannot transport Fe²⁺. In contrast to the WT IRT1 protein, both IRT1_{S206A} and IRT1_{H232A} failed to complement the growth impairment of an Fe uptake-defective *S. cerevisiae* *fet3fet4* mutant on low-Fe media (Figure 4(a)), as reported previously (Rogers et al., 2000). In order to obtain *in planta* evidence, we quantified ⁵⁵Fe²⁺

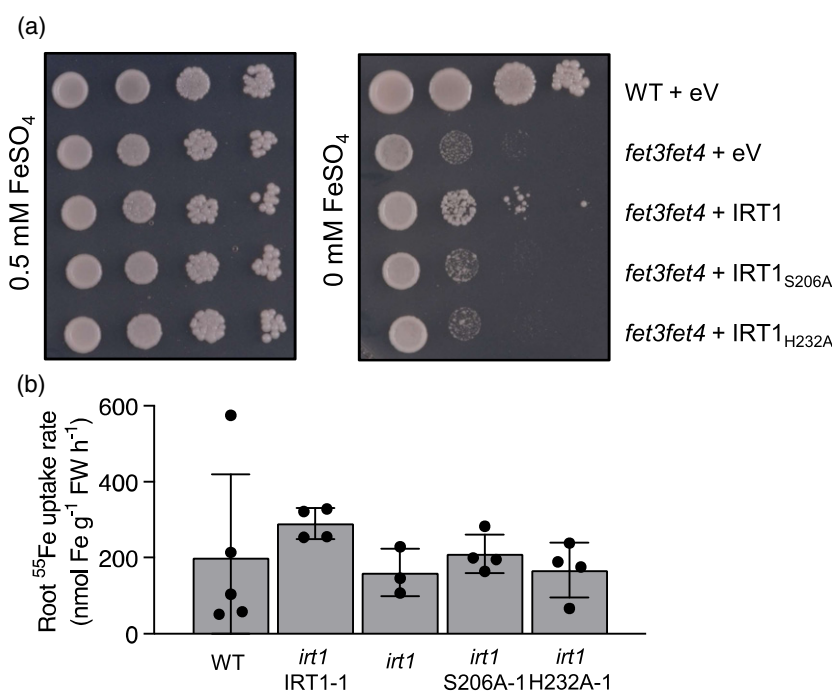
incorporation into roots of approximately 8-week-old hydroponically cultivated WT, *irt1*, *irt1* IRT1, *irt1* S206A and *irt1* H232A plants after exposure to Fe deficiency for a period of 6 days. Short-term uptake rates of ⁵⁵Fe²⁺ into roots were not decreased in *irt1* by comparison to the WT (Figure 4(b), Table S2). This result was contrary to expectations, given the lack of the high-affinity root Fe²⁺ uptake system in the *irt1* mutant, and it precluded the complementation testing that we had intended to achieve with this experiment. Importantly, we also detected no differences in root ⁵⁵Fe²⁺ uptake rates between *irt1* S206A and *irt1* H232A, indicating against the differential activation of any secondary Fe uptake systems as the cause for their differing phenotypes (Figure 4(b)). Altogether, these results suggest that roots of mutants lacking IRT1 transport activity retain significant root Fe²⁺ uptake rates under the employed conditions, which is counter-intuitive but consistent with previously published results including one short-term and one longer-term radiotracer uptake experiment (Henriques et al., 2002; Vert et al., 2002).

The root-to-shoot Fe partitioning defect of *irt1* is partially rescued by the transport-inactive IRT1_{S206A} variant

We observed root Fe overaccumulation in *irt1*, as well as a partial complementation of growth impairment and chlorosis of *irt1* by a transport-inactive IRT1_{S206A} mutant (see Figures 1(c), 2 and 3). Next we addressed root-to-shoot Fe partitioning. Shoot Fe concentrations were significantly higher in *irt1* S206A lines compared to *irt1* following growth in control media, and indistinguishable from *irt1* in *irt1* H232A (Figure 5(a,b)). Note that all three of these

Figure 4. Yeast complementation assay and root ⁵⁵Fe²⁺ uptake rates.

(a) Growth of WT and the *fet3fet4* Fe transport-defective mutant transformed with a modified pFL61 plasmid as empty vector (eV), or containing the IRT1, IRT1_{S206A} or IRT1_{H232A} cDNA, respectively. Ten-fold serial dilutions of liquid cultures were spotted on SD (-Ura) medium (pH 5.7) supplemented with 0.5 mM FeSO₄ or left unamended. (b) Uptake rates determined in hydroponically cultivated 7.5- to 8.5-week-old plants over a 13.5-min period. Before the initiation of uptake assays, plants were exposed to Fe deficiency (0 μM FeHBED) for 6 days, subsequent to an initial cultivation period in 1× modified Hoagland's solution containing 10 μM FeHBED (WT and *irt1* IRT1) or 50 μM FeHBED (all other genotypes) for 6 to 7 weeks. Bars represent arithmetic mean ± SD (*n* = 4 to 5 plants). Data show one experiment representative of three independent experiments (see Table S2).



genotypes are physiologically more Fe-deficient than WT in control media, based on classical Fe deficiency markers (Vert et al., 2002; Figure 3(c), Figure S4(a)), because they share the lack of IRT1-mediated high-affinity root Fe uptake. Upon growth on Fe-deficient media, there was little or no difference in shoot Fe concentrations between WT and *irt1* (as noted before, see Figure 1), indicating that this condition is generally less informative (Figure 5(a,b)). Fe allocation to shoots corroborated a partial complementation in *irt1* S206A lines of the root-to-shoot Fe partitioning defect of *irt1* (Figure 5(c,d)). Shoot Mn concentrations were in agreement with the lack of active IRT1 protein in the

roots, because the levels of Mn – as a secondary substrate of IRT1 – were similar in shoots of the *irt1* mutant and the transport-inactive lines (Figure 5(e,f)). Different from Mn concentrations, the concentrations of Zn and Cu were increased in shoots of *irt1* and unchanged in roots of *irt1*, suggesting that transport proteins other than IRT1 make a predominant contribution to the accumulation of Zn and Cu under our cultivation conditions (Figure S6).

Root Fe accumulation of *irt1* mutants was restored down to levels resembling the WT in *irt1* S206A seedlings, but not in *irt1* H232A, under control conditions (Figure 6(a,b), Figure S7). Note that *irt1* IRT1 lines contained higher IRT1

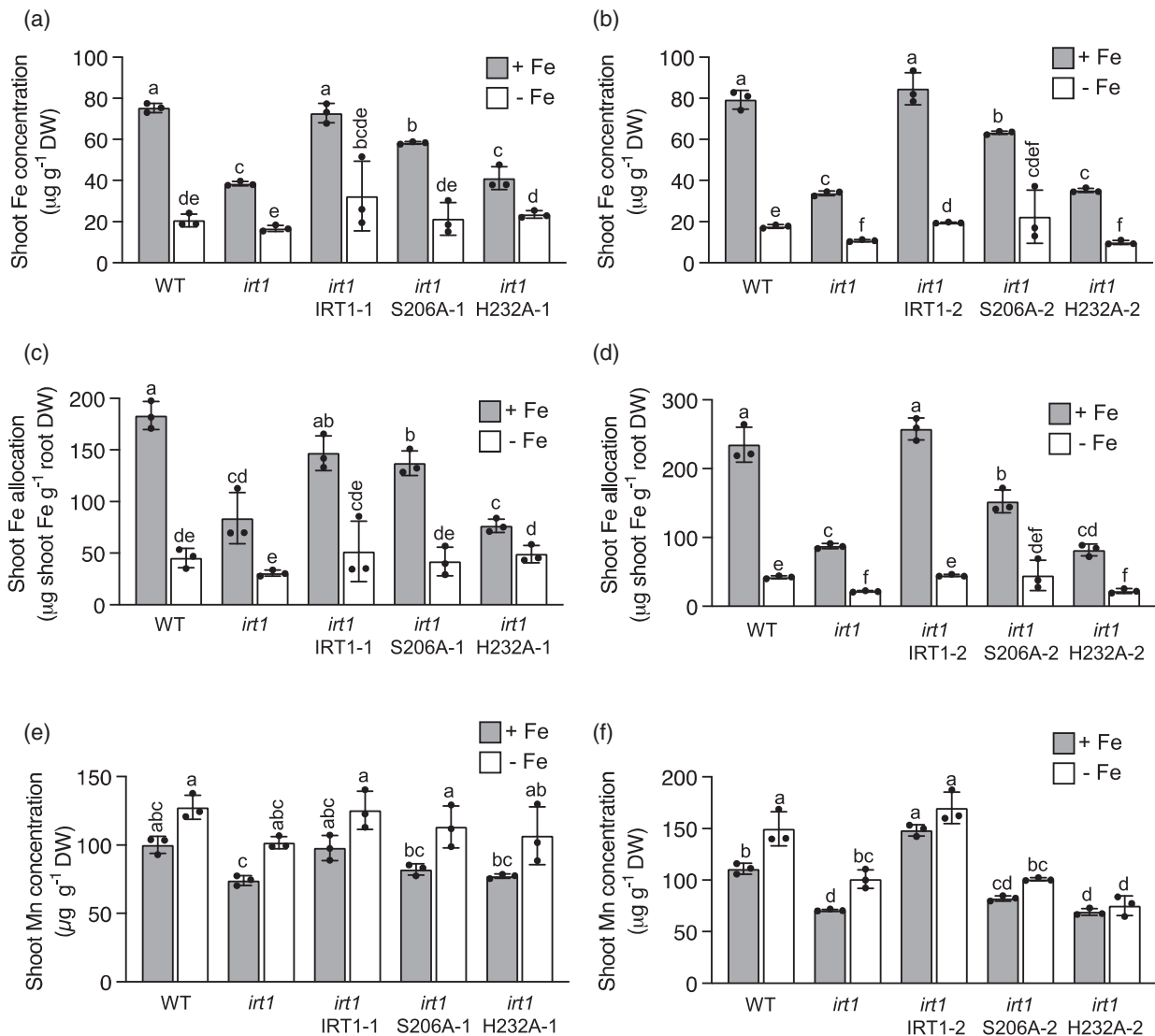


Figure 5. Partial rescue of root-to-shoot Fe allocation in *irt1* S206A.

(a–f) Shoot Fe concentrations (a and b), shoot Fe allocation (c and d) and shoot Mn concentrations (e and f) in 20-day-old seedlings of WT, *irt1*, *irt1* IRT1, *irt1* S206A and *irt1* H232A grown on Fe-sufficient (+Fe, 10 µM FeHBED) and Fe-deficient (–Fe, 0 µM FeHBED) agar-solidified 0.25× modified Hoagland's medium (EDTA-washed agar) for 10 days, subsequent to an initial cultivation period of 10 days in standard medium (5 µM FeHBED; unwashed agar), on vertically oriented Petri plates. Bars represent arithmetic mean ± SD ($n = 3$ pools of tissues, each from 15 to 30 seedlings, with 15 seedlings cultivated per plate). Distinct letters indicate significant differences ($P < 0.05$) according to two-sample Student's t -tests upon correction for multiple comparisons (a–d) or in two-way ANOVA followed by Tukey's HSD test (e and f). Data show one experiment representative of two independent experiments.

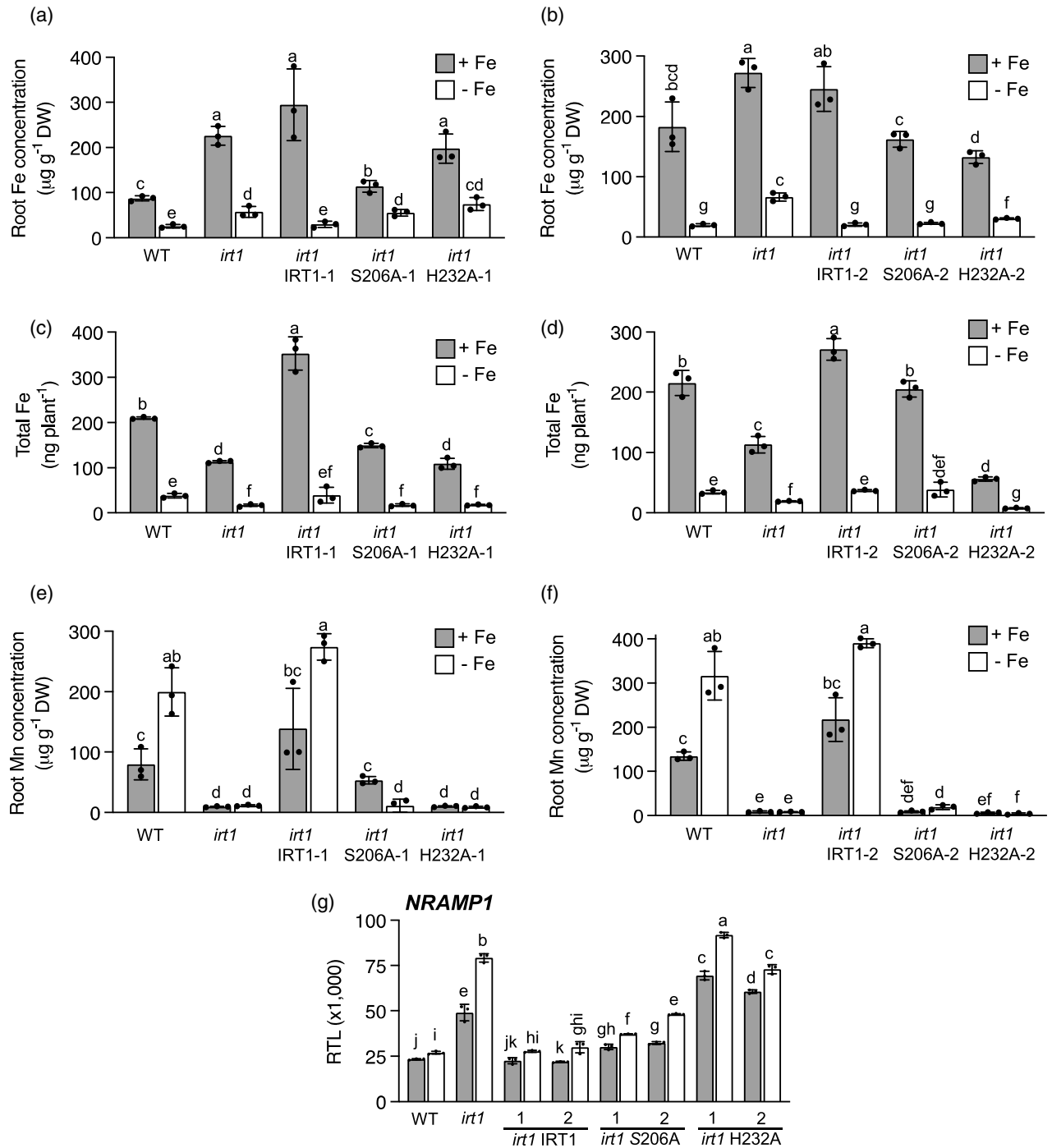


Figure 6. Root Fe concentrations, total Fe per plant, root Mn concentrations, and *NRAMP1* expression.

(a–f) Root Fe concentrations (a and b), total Fe per plant (c and d) and root Mn concentrations (e and f) in 20-day-old seedlings of WT, *irt1*, *irt1* IRT1, *irt1* S206A and *irt1* H232A grown on Fe-sufficient (+Fe, 10 μM FeHBED) and Fe-deficient (–Fe, 0 μM FeHBED) agar-solidified 0.25 \times modified Hoagland's medium (EDTA-washed agar) for 10 days, subsequent to an initial cultivation period of 10 days in standard medium (5 μM FeHBED; unwashed agar), on vertically oriented Petri plates. (g) *NRAMP1* relative transcript levels (RTLs) in 15-day-old seedlings of WT, *irt1* and various transgenic *irt1* lines grown on +Fe and –Fe medium for 5 days. Transcript levels are shown normalized to those of *UBQ10* and *EF1 α* . Bars represent arithmetic mean \pm SD ($n = 3$ pools of tissues from 15 to 30 seedlings, with 15 seedlings cultivated per plate (a–f); $n = 3$ technical replicates on cDNA obtained using tissue pooled from 2 to 3 plates, each with 20 seedlings) (g). Distinct letters indicate significant differences ($P < 0.05$) according to two-sample Student's *t*-tests upon correction for multiple comparisons. Data show one experiment representative of two (a–f) or four (g) independent experiments.

transcript and IRT1 protein levels than the WT under +Fe conditions (see Figure S4(b)), which affects Fe homeostasis, and that *irt1* H232A seedlings of line 2 were very small and chlorotic (see Figure 3). Total Fe per plant in the *irt1* H232A lines was similar to (*irt1* H232A-1), or even lower (*irt1* H232A-2) than, total Fe in the *irt1* mutant. In *irt1* S206A lines, total Fe was consistently higher than total Fe of *irt1* and the *irt1* H232A lines, and lower than, or similar to, that of WT and *irt1* IRT1, in control conditions (Figure 6(c,d)). We propose that increased total Fe levels in the *irt1* S206A lines could be attributed to larger seedling size, a larger root surface area resulting from a longer root in *irt1* S206A than in *irt1* (see Figure 3), or differing overall Fe homeostasis as a consequence of altered Fe distribution within the plant. In *irt1*, *irt1* S206A and *irt1* H232A, root concentrations of the secondary IRT1 substrate Mn were generally far lower than in both WT and *irt1* IRT1 seedlings, in which they increased under -Fe with increasing IRT1 protein levels, as expected (see Figure 6). In *irt1* S206A-1, root Mn concentrations were 35% lower than WT levels, but not statistically detected as significantly different from the WT. The fact that root Mn concentrations did not increase at all on -Fe medium in the presence of increased levels of IRT1_{S206A} protein (compare Figure 6(e) with Figure 3(a)) suggested against a direct causal involvement of IRT1_{S206A} in the slightly elevated root Mn concentrations of *irt1* S206A line 1. Therefore, we interpret this as a line-specific effect unrelated to IRT1 (compare with *irt1* S206A line 2, Figure 6(f)). These results indicate that the IRT1_{S206A} and IRT1_{H232A} variants are incapable of mediating IRT1-dependent and Fe deficiency-enhanced root accumulation of the secondary IRT1 substrate Mn²⁺ *in planta*. By extension, it is unlikely that these two variants are capable of Fe²⁺ transport *in planta*. Root *NRAMP1* transcript levels were 2- to 3.3-fold elevated in *irt1* and *irt1* H232A lines, when compared to the WT (Figure 6(g)). In *irt1* S206A they were lower than in *irt1* and remained only slightly, between 1.3- and 1.8-fold, increased compared to *NRAMP1* transcript levels of the WT and *irt1* IRT1 lines. These observations are consistent with IRT1 being the predominant membrane transport protein contributing to root Mn levels under our experimental conditions. Taking these results together, residual IRT1 transport activity or an activation of a secondary Fe uptake system, including *NRAMP1*, cannot explain the partial complementation of shoot Fe levels in *irt1* S206A lines (see Figure 5(a,b)). In summary, the root-to-shoot Fe partitioning defect of the *irt1* mutant is partially rescued by the transport-inactive IRT1_{S206A}, but not by IRT1_{H232A}.

Ferritins are plastid-localized Fe storage proteins, and their levels increase when plants are Fe-replete (Briat et al., 2009). In shoots of WT and *irt1* IRT1 seedlings cultivated on -Fe media for 5 days, *FERRITIN1* (*FER1*) transcript levels were as low as 4.6 to 6.7% of those observed in control media (Figure 7(a)). *FER1* expression in *irt1* H232A

under control conditions was comparable to that of *irt1* and Fe-deficient WT (Figure 7(a)). *FER1* transcript levels in shoots of *irt1* S206A lines were intermediate between WT and *irt1*, in agreement with growth and Fe contents in these lines (Figure 7(a), compare Figure 5 and Figure 6). In roots, the differences in *FER1* transcript levels between lines were qualitatively similar, but quantitatively much smaller, in line with root Fe levels (Figure 7(b), compare Figure 5 and Figure 6). Transcript levels of Fe deficiency marker genes *IRONMAN1* (*IMA1*), *ZINC INDUCED FACILITATOR1* (*ZIF1*), *bHLH39* and *NAS4* in shoots further corroborated a partial complementation of *irt1* by IRT1_{S206A}, as evident upon cultivation in control media (Figure S8).

How is Fe homeostasis altered in roots of *irt1*?

We examined whether Fe status marker genes can additionally provide insights into Fe homeostasis in the *irt1*

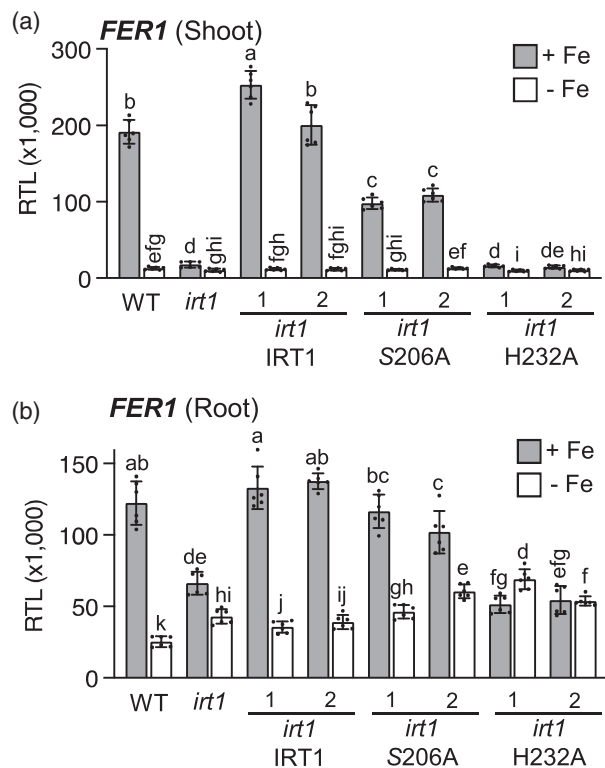


Figure 7. *FER1* transcript levels.

(a–c) Relative transcript levels (RTLs) of *FER1* in shoots (a) and roots (b) of 15-day-old WT, *irt1*, *irt1* IRT1, *irt1* S206A and *irt1* H232A seedlings. RTLs are shown normalized to both *UBQ10* and *EF1α* as constitutively expressed control genes. Seedlings were grown on Fe-sufficient (+Fe, 10 μM FeHBED) and Fe-deficient (-Fe, 0 μM FeHBED) agar-solidified 0.25× modified Hoagland's medium (EDTA-washed agar) for 5 days, subsequent to an initial cultivation period of 10 days in standard medium (5 μM FeHBED; unwashed agar), on vertically oriented Petri plates. Bars represent arithmetic mean ± SD ($n = 6$ technical replicates on cDNA obtained using tissue pooled from 2 to 3 plates, each with 20 seedlings). Distinct letters indicate significant differences ($P < 0.05$) according to two-sample Student's or Welch t -tests upon correction for multiple comparisons. Data show one experiment representative of three independent experiments.

mutant and thus into possible secondary functions of the IRT1 protein. According to all the marker genes analyzed, the degree of physiological Fe deficiency in shoots of the *irt1* mutant grown in control media was approximately equivalent to, or slightly more severe than, that in the WT after 5 days of cultivation on Fe-deficient media (Figure 7, Figure S8). Note that we quantified biomass and mineral contents of tissues after 10-day treatments in order to avoid experimental noise from low biomass of some samples and the associated sensitivity of our results to contamination, for example from dust particles. Considering roots, *FER1* transcript levels in Fe-deficient WT and *irt1* IRT1 seedlings were 20 to 28% of those observed in Fe-replete media (Figure 7(b)). When compared to the WT, *FER1* transcript levels in roots of the *irt1* mutant were reduced to a clearly lesser extent than in shoots after cultivation under control conditions. However, root *FER1* transcript levels did not fully reflect increased root Fe concentrations in *irt1* compared to the WT (compare Figure 7(b) with Figures 1(c) and 2(a)). *FER1* transcript levels are highly localized in 7-day-old seedlings according to the eFP browser, with at least 3.5 times higher *FER1* transcript levels in root endodermal and phloem companion cells and at least 2.5 times higher *FER1* transcript levels in root pericycle cells than in root cortex and epidermal cells (Figure S12(a)) (Brady et al., 2007; Winter et al., 2007). All in all, these results suggest a more Fe-replete status in roots than in shoots of *irt1*, supporting that root-accumulated Fe is at least partly physiologically accessible and thus intracellular in the *irt1* mutant.

Additional genes of the root Fe deficiency response are mis-regulated in *irt1*

Next we addressed transcriptome differences between *irt1* and the WT in order to identify candidate genes for mediating decreased root-to-shoot Fe mobility in the *irt1* mutant. Between 3 and 5 days of Fe deficiency were previously shown to result in maximal transcriptional responses in roots (Connolly et al., 2002, 2003; Vert et al., 2003). In our experimental conditions, root surface Ferric Chelate Reductase (FCR) activity in WT seedlings reached a maximum at 5 days of Fe deficiency (Figure S9(a)). At the time point selected for harvest, FCR activity of the *irt1* mutant was 3.2-fold higher than that of WT under control conditions (+Fe; Figure S9(b)). In the WT, FCR activity was 6.6-fold higher under –Fe than under +Fe conditions and approximately 2-fold higher than in the *irt1* cultivated on +Fe medium (Figure S9(b)). Thus, the systemic activation and deactivation of Fe deficiency responses in roots dependent on shoot Fe status is functional in *irt1* (Vert et al., 2003).

We conducted microarray-based transcriptomics in 15-day-old WT and *irt1* seedlings grown in Fe-replete media (+Fe) as well as WT seedlings cultivated in Fe-deficient (–Fe) media for the final 5 days before harvest (see also

previous section). A comparison between –Fe and +Fe conditions in WT seedlings identified the transcriptomic Fe deficiency response under our experimental conditions (–Fe versus C (WT)). The comparison between *irt1* and WT cultivated under +Fe conditions identified all symptoms and consequences of the lack of IRT1 (*irt1* versus WT (C)). Finally, we compared between *irt1* cultivated under +Fe conditions and WT cultivated under –Fe conditions to identify transcriptome aberrations in the *irt1* mutant (*irt1* (C) versus WT –Fe) (Figure S9(c)).

In our transcriptomics attempt to identify candidate genes for altered root-to-shoot Fe partitioning in the *irt1* mutant, we expected that candidate gene transcript levels respond to Fe deficiency conditions in the WT because IRT1 protein levels respond to Fe deficiency conditions. IRT1 is expressed in roots, and roots are the primary organ that governs root-to-shoot translocation of mineral nutrients. Among the transcripts of which levels increased more than 2-fold under –Fe compared to control conditions in WT roots, 44% had higher levels in *irt1* than WT under control conditions (Figure 8(a), –Fe versus C (WT) ↑ and *irt1* versus WT (C) ↑). Approximately three-quarters of these transcripts increased in abundance in *irt1* similarly to the increase in Fe-deficient WT (Table 1 and Data S2). But for the remaining 26% of these transcripts, this increase was clearly less pronounced than expected from the physiological Fe status of *irt1* plants (Figure 8(a), Table 1 and Figure S10, *irt1* versus WT (–Fe) ↓, marked by a single asterisk; see above). This group of 20 genes comprises candidates for an IRT1-dependent function in root-to-shoot partitioning of Fe. The corresponding genes included a number of functionally uncharacterized or poorly characterized genes, as well as previously characterized Fe homeostasis genes including *MYB72*, *IMA1*, *bHLH101*, *NAS4* and *BETA-GLUCOSIDASE42 (BGLU42)*, for example (Data S1; note that *bHLH100* and *bHLH38*, which are similar to *bHLH101* in both sequence and biological function, are not represented on the microarray). Of the transcripts that decreased in abundance under –Fe versus C (WT) and also in *irt1* versus WT (C), none were under-responsive in *irt1* (Figure 8(b)).

A severe de-regulation in the *irt1* mutant was apparent for a total of 43 Fe deficiency-responsive transcripts of WT, which were not significantly regulated in the same direction in *irt1* versus WT (C), and thus showed an unexpected non-responsiveness in *irt1*. These more promising candidate genes for an IRT1-dependent function in root-to-shoot Fe partitioning included *MYB10* and *CYTOCHROME P450 71B5 (CYP71B5)* (up in WT –Fe), as well as *BETA-GLUCOSIDASE45 (BGLU45)* and *LACCASE7 (LAC7)* (down in WT –Fe), for example (Figure 8(a,b), Table 1 and Figure S10, double asterisks; Data S1). Transcript levels of *MYB10* and *CYP71B5* are known to respond strongly to Fe deficiency (Buckhout et al., 2009; Yang et al., 2010).

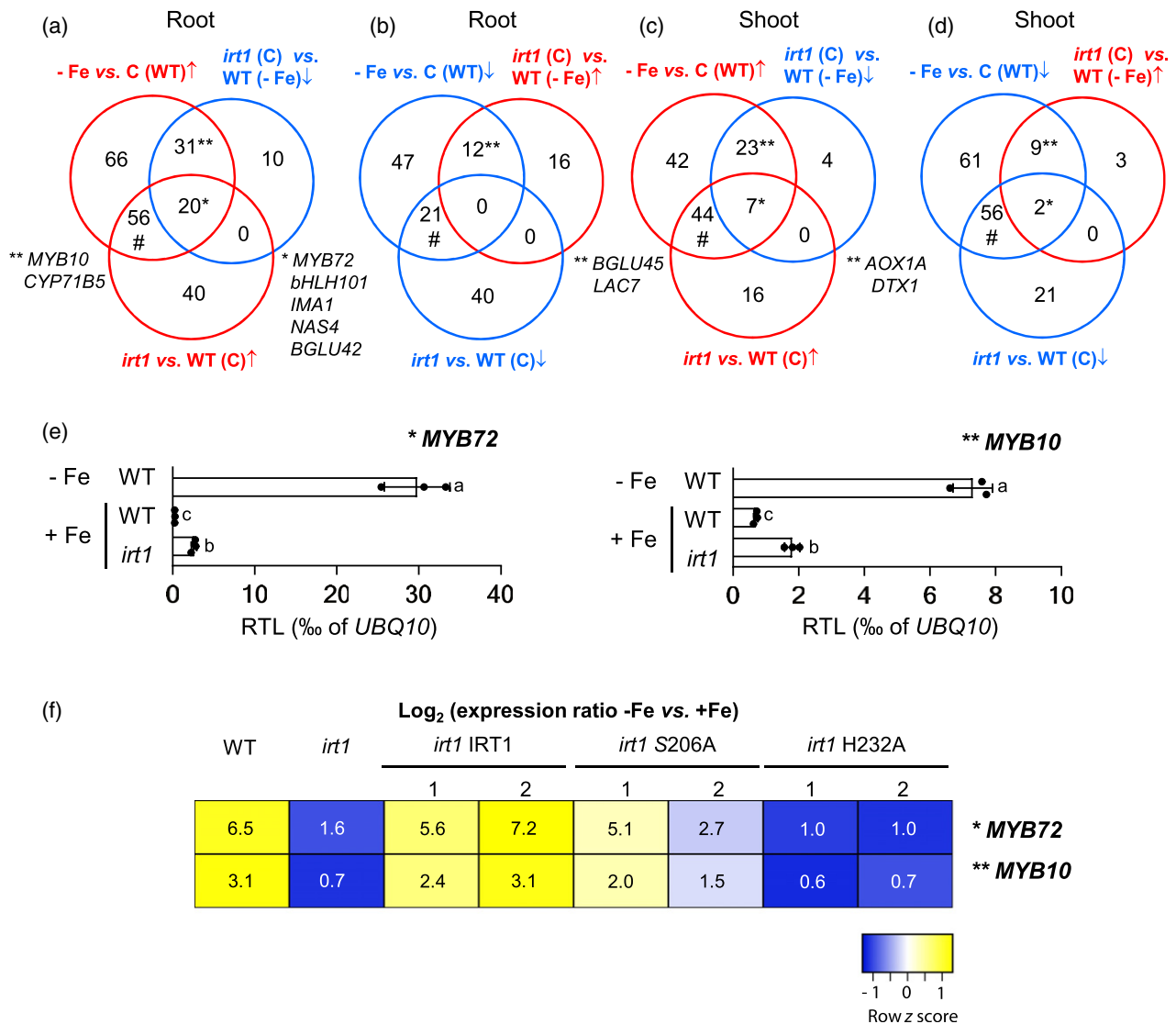


Figure 8. Transcriptome analysis of *irt1* compared to Fe-deficient and -sufficient WT seedlings. (a–d) Summary of microarray-based transcriptome data in roots (a and b) and shoots (c and d). Shown within Venn diagrams are the numbers of genes with ≥ 2 -fold differences in transcript levels in different comparisons ($P < 0.15$). Colors denote responses (red/blue, higher/lower transcript abundance in one genotype and/or condition compared to the other). Symbols denote Fe deficiency-responsive transcripts that are de-regulated (*, **) or not (#) in *irt1*. (e) Relative transcript levels (RTLs) of *MYB10* and *MYB72* in roots of WT and *irt1* seedlings. RTLs are shown normalized to *UBQ10*. (f) Heatmap of *MYB72* and *MYB10* transcript abundance under -Fe versus +Fe conditions in roots of different genotypes as indicated. Numbers are \log_2 (transcript level ratios, with RTL normalized to both *UBQ10* and *EF1 α*) values, and the raw z-score for each gene was used to scale the heatmap, from three independent experiments. WT and *irt1* seedlings were grown on Fe-sufficient (+Fe, 10 μM FeHBED) and Fe-deficient (-Fe, 0 μM FeHBED) agar-solidified modified 0.25 \times Hoagland's medium (EDTA-washed agar) for 5 days, subsequent to an initial cultivation period of 10 days in standard medium (5 μM FeHBED; unwashed agar), on vertically oriented Petri plates (a–f). Bars represent arithmetic mean \pm SD ($n = 3$ technical replicates on cDNA obtained using tissue pooled from 2 to 3 plates, each with 20 seedlings (e)). Distinct letters indicate significant differences ($P < 0.05$) in two-way ANOVA followed by Tukey's HSD test (*MYB10*) or two-sample Student's *t*-tests upon correction for multiple comparisons (*MYB72*). Data in (f) are from three independent experiments.

BGLU45 and *LAC7* are thought to function in cell wall lignification (Chapelle et al., 2012; Schulten and Krämer, 2017).

We cannot exclude that causative genes may act in shoots, given that *IRT1* expression in phloem companion cells was reported to be critical for its *in planta* function (Marquès-Bueno et al., 2016). In shoots, 76 and 71% of the transcripts that differed in abundance in *irt1* compared to WT under control conditions were also up- or

downregulated, respectively, when WT was exposed to Fe deficiency (Figure 8(c), *irt1* versus WT (C) \uparrow and -Fe versus C (WT) \uparrow ; Data S4). Again, some of those transcripts were not up- or downregulated as expected in Fe-deficient *irt1*, e.g., *ALTERNATIVE OXIDASE1* (*AOX1A*) or *DETOXIFICATION1* (*DTX1*) (Figure 8(c,d), double asterisks; Data S3).

In an independently cultivated experiment, compared to +Fe, the levels of the root-specific transcript *MYB72* were

Table 1 Responses of canonical Fe deficiency-responsive transcripts in –Fe versus C (WT) and *irt1* versus WT (C)

Gene model AGI code	Other names	Fold change –Fe versus C (WT)		Direction	Fold change <i>irt1</i> versus WT (C)		Direction
		Microarray	qPCR		Microarray	qPCR	
De-regulated in <i>irt1</i> (*, **, see Figure 8 (a-d))							
Roots							
AT4G19690	<i>IRT1</i> ^a	16.1	20.8	up	17.9	4.6	down
AT3G53280	<i>CYP71B5</i> ^b	23.3	48.7	up	1.7 ns	3.4	up
AT4G19680	<i>IRT2</i> ^c	22.7	22.4	up	2.0	1.0	up
AT3G12820	<i>MYB10</i> ^b	10.8	9.7	up	3.0 ns	3.9	up
AT4G31940	<i>CYP82C4</i> ^b	75.4	n/a	up	36.3	n/a	up
AT1G56160	<i>MYB72</i> ^b	53.2	197.7	up	3.8	22.1	up
AT3G12900	<i>S8H</i> ^p	43.9	n/a	up	14.3	n/a	up
AT1G47400	<i>IMA1</i> ^d	41.9	24.6	up	11.8	12.4	up
AT5G04150	<i>bHLH101</i> ^e	24.3	37.8	up	10.5	9.0	up
AT1G56430	<i>NAS4</i> ^f	9.6	27.1	up	3.0	15.2	up
AT5G36890	<i>BGLU42</i> ^b	7.9	10.1	up	2.3	1.8	up
AT3G09220	<i>LAC7</i>	4.2	3.3	down	1.4 ns	1.8	down
AT4G23700	<i>CHX17</i> ^g	2.7	n/a	down	1.1 ns	n/a	up
Not de-regulated in <i>irt1</i> (#, see Figure 8(a-d))							
Shoots							
AT1G47400	<i>IMA1</i> ^d	126.8	57.2	up	83.1	76.04	up
AT3G56980	<i>bHLH39</i> ^e	115.3	332.73	up	79.1	261.46	up
AT5G04150	<i>bHLH101</i> ^e	61.2	n/a	up	59.9	n/a	up
AT1G23020	<i>FRO3</i> ^g	9.9	n/a	up	6.9	n/a	up
AT3G18290	<i>BTS</i> ^d	9.0	n/a	up	7.3	n/a	up
AT4G16370	<i>OPT3</i> ^g	7.6	n/a	up	6.3	n/a	up
AT1G56430	<i>NAS4</i> ^f	7.6	9.2	up	5.3	6.8	up
AT5G13740	<i>ZIF1</i> ^h	6.2	11.2	up	4.8	11.8	up
AT3G47640	<i>PYE</i> ^d	4.8	n/a	up	3.8	n/a	up
AT5G67330	<i>NRAMP4</i> ⁱ	3.8	n/a	up	3.5	n/a	up
AT4G25100	<i>FSD1</i> ^j	120.5	n/a	down	77.7	n/a	down
AT5G01600	<i>FER1</i> ^k	33.8	14.9	down	32.0	10.7	down
AT2G40300	<i>FER4</i> ^k	17.8	n/a	down	20.8	n/a	down
AT1G76800	<i>VTL2</i> ^l	4.7	n/a	down	3.4	n/a	down
AT1G09240	<i>NAS3</i> ^g	4.3	n/a	down	3.8	n/a	down
AT4G24120	<i>YSL1</i> ^m	3.9	n/a	down	3.2	n/a	down
AT3G56090	<i>FER3</i> ^k	3.9	n/a	down	4.1	n/a	down
AT3G25190	<i>VTL5</i> ^d	3.2	n/a	down	2.6	n/a	down
Roots							
AT3G56980	<i>bHLH39</i> ^e	39.2	55.9	up	21.3	21.3	up
AT4G16370	<i>OPT3</i> ^g	17.3	n/a	up	8.9	n/a	up
AT3G58810	<i>MTP3</i> ^b	15.5	n/a	up	10.7	n/a	up
AT3G46900	<i>COPT2</i> ^b	14.9	n/a	up	7.7	n/a	up
AT1G23020	<i>FRO3</i> ^g	9.8	n/a	up	5.2	n/a	up
AT5G03570	<i>FPN2</i> ^b	8.1	n/a	up	4.7	n/a	up
AT1G74770	<i>BTSL1</i> ^d	6.9	5.6	up	3.7	2.5	up
AT2G28160	<i>FIT</i> ^b	3.8	2.1	up	2.4	1.4	up
AT4G33020	<i>ZIP9</i> ^b	3.3	n/a	up	2.5	n/a	up
AT5G01600	<i>FER1</i> ^k	9.2	4.8	down	4.9	1.8	down
AT4G25100	<i>FSD1</i> ^j	7.5	n/a	down	5.0	n/a	down
AT1G21140	<i>VTL1</i> ^d	6.4	n/a	down	3.7	n/a	down
AT2G40300	<i>FER4</i> ^k	4.9	n/a	down	3.2	n/a	down
AT1G76800	<i>VTL2</i> ^l	3.2	n/a	down	3.0	n/a	down
AT3G56090	<i>FER3</i> ^k	3.0	n/a	down	2.2	n/a	down

Genes shown are subsets of those represented in Figure 8(a–d) and Data S1–S4. ns: non-significant in microarray analysis; n/a: not analyzed. References: ^aEide et al., 1996; ^bColangelo and Guerinot, 2004; ^cVert et al., 2001; ^dBuckhout et al., 2009; ^eWang et al., 2007; ^fBauer et al., 2004; ^gWintz et al., 2003; ^hHaydon et al., 2012; ⁱThomine et al., 2000; ^jWaters et al., 2012; ^kPetit et al., 2001; ^lGollhofer et al., 2014; ^mLe Jean et al., 2005.

(*,***) refers to the symbols exactly as used in Figure 8 (a-d). It thus refers back to the classification of genes according to their regulation in Fig. 8.

upregulated approximately 100-fold in –Fe-grown WT, but in *irt1* they reached only about 8% of the transcript levels in –Fe-grown WT according to our reverse transcription quantitative real-time PCR (RT-qPCR) analysis, thus fully confirming the microarray data (Figure 8(e)). For *MYB10*, a 10-fold increase in transcript levels was observed in the WT in –Fe, whereas the increase in *irt1* was only about 2.6-fold (Figure 8(e), compare with 3-fold change, not statistically significant, according to the microarrays). The *CYP71B5* expression profile was similar to that of *MYB10* and *MYB72* (Figure S11(a,e)). Thus, according to RT-qPCR, *MYB10* and *CYP71B5* also form part of the regulatory category represented by *MYB72*, so that the microarrays may have been insufficiently sensitive to detect this (Figure 8(a), *). RT-qPCR also suggested that the *bHLH39* expression ratio between *irt1* and –Fe-grown WT was 2.7, whereas the microarray data had suggested a ratio below 2 (Figure 8(a), #; Figure S11(b,e)). Both microarray and RT-qPCR results supported that root transcript levels of *CYP71B5* were severely under-responsive, and those of *bHLH39* were considerably more responsive, to the general Fe deficiency in *irt1* seedlings. In shoots, fully confirming the microarray data, RT-qPCR detected no statistically significant difference in transcript levels of *NAS4* between WT –Fe and *irt1* +Fe (Figure S11(d,e)). Transcript levels of *DTX1*, however, in *irt1* were only about 16% of those in WT –Fe (Figure S11(c,e)), also confirming the microarray data. Thus, in shoots of *irt1*, *DTX1* transcript levels did not follow the physiological Fe status, whereas *NAS4* transcript levels did.

There are some complexities affecting the identification of candidate genes for a role in IRT1-dependent root-to-shoot Fe partitioning. As detailed above, the de-regulation of expression of Fe deficiency-responsive genes in the *irt1* mutant could well constitute the cause of altered Fe partitioning in the *irt1* mutant, such that these genes contribute to the mechanism. Alternatively, the de-regulation of gene expression in *irt1* could merely be a consequence of the locally altered physiological status of Fe or of secondary substrate metals in the *irt1* mutant by comparison to the WT, or of the differing dynamics of Fe deficiency responses in *irt1* and the WT over time. Complicating this even further, the cell-autonomous, non-cell-autonomous or even systemic contributions of the transcriptional regulation of these genes have not been established yet. Finally, the cell type specificity of candidate gene expression in relation to Fe localization were not considered in our transcriptomics experiment.

To begin to tackle this latter issue, we next attempted to employ information from publicly available cell type-specific gene expression data. Using the GEO2R tool and available cell-type specific datasets (GEO; <https://www.ncbi.nlm.nih.gov/geo/>, GSE10501), we identified transcripts that are at least 2-fold more abundant either in the cortex

or in the endodermis than in the stele under conditions of –Fe (24 h treatment) (Dinnyen et al., 2008). Among these genes, we then focused on the subgroup of genes for which our data indicated differential transcript abundance in WT roots between –Fe and +Fe conditions, as putative reporters of local Fe status (Data S5 and S6). However, the expression of many of these genes is likely to be systemically controlled according to the Fe status of the shoot, like *IRT1* (Vert et al., 2003). Therefore, among the chosen genes, we finally identified those genes as putative markers of local Fe status, of which transcript levels in *irt1* followed Fe distribution across its roots (see Figure 1(b)), i.e., did not suggest a more deficient physiological Fe status in *irt1* versus WT roots under control conditions. Expression of 38 Fe deficiency-responsive genes is higher in the cortex than in the stele, including *BGLU45*, *ZRT/IRT-LIKE PROTEIN2 (ZIP2)*, *NAS1*, *AT3G43670* and *BTSL2*, for example (Dinnyen et al., 2008). Additionally, their transcript levels did not show a statistically significant Fe deficiency response in *irt1* compared to WT under control conditions, according to our microarray data from bulk root tissues (Data S5). We confirmed this by RT-qPCR for *BGLU45* and *BTSL2* (Figure S12). Given that published data from promoter-GUS fusions of *BTSL2* (Rodríguez-Celma et al., 2019) rather suggest a broad expression domain in Fe-deficient roots, the most promising marker transcript that may reflect local Fe status in root cortex cells remains *BGLU45*, encoding beta-glucosidase 45.

Candidate genes for roles in IRT1-dependent root-to-shoot Fe partitioning

We identified a group of Fe deficiency-responsive genes as under-responsive in roots of the *irt1* mutant (Figure 8, * and **; Data S1 and S2). Among these, we identified *MYB72* and *MYB10* as candidates for putative roles in IRT1 protein-dependent root-to-shoot Fe translocation, for example. Therefore, we analyzed transcript levels of *MYB72* and *MYB10* across our panel of transgenic lines, following cultivation as for microarray-based transcriptomics. Indeed, roots of *irt1* S206A lines responded to Fe deficiency, compared to control conditions, with a larger increase of *MYB72* and *MYB10* expression than in *irt1* and *irt1* H232A (Figure 8(f); Figure S13). Additional candidate genes that are also Fe status markers, *NAS4* and *IMA1*, exhibited a similar expression pattern (Figure S13). These observations can be interpreted as a partial complementation of an attenuated Fe deficiency responsiveness in *irt1* roots (see Figure 8). Different from *irt1* S206A, changes in transcript levels between Fe-deficient and Fe-replete conditions suggested that the response of *irt1* H232A to Fe levels in the media was overall similarly attenuated as in the *irt1* mutant (Figure 8). Together, these results are consistent with possible roles of the transcription factor-coding genes *MYB72* and *MYB10* as well as their target gene *NAS4*, and

IMA1, in IRT1-dependent root-to-shoot Fe partitioning, but further work will be required to obtain unequivocal evidence for such a role of these or other candidate genes.

DISCUSSION

High root Fe concentrations in the *irt1* mutant

Our results indicate that roots of the *irt1* mutant accumulate Fe (Figures 1, 2 and 6, Figures S2 and S7). By contrast, shoots of the *irt1* mutant – as is well established and confirmed again here – contain reduced Fe concentrations as long as Fe is not growth-limiting, compared to the WT (Figures 1 and 5). Several earlier studies suggested that the *irt1* mutant may contain unexpectedly high levels of Fe in the root, but the physiological significance of this had remained unaddressed (Cailliatte et al., 2010; Henriques et al., 2002; Ivanov et al., 2014). Indeed, the use of EDTA as a chelator of Fe³⁺ in the synthetic media of these studies favored the precipitation of Fe (Becher et al., 2004; Chaney, 1988; Salomé et al., 2014) and consequently the authors very appropriately considered that an incomplete desorption of apoplastically precipitated or bound Fe could have affected their results. In this study, the use of HBED as Fe³⁺ chelator in combination with a comparably low total Fe concentration is better suited for maintaining Fe³⁺ in solution in a synthetic medium. In line with this, Fe concentrations in roots remained in the range of those in shoots of the WT (Figure 1(d)). The *irt1-2* mutant used here fails to express both *IRT1* and *IRT2* (Figure S4). An involvement of *IRT2* in the phenotypes of *irt1-2* reported here is unlikely because these phenotypes were primarily evident under +Fe cultivation conditions, under which *IRT2* transcript levels were extremely low in both WT and *irt1-2*. Note that in roots of WT seedlings, relative *IRT2* transcript levels were less than 6.5 and 6.1% of those of *IRT1* upon cultivation in –Fe and +Fe medium, respectively (Figure S4(a)). Additionally, compared to *irt1*, *IRT2* transcript levels were not elevated in the complementing *irt1* IRT1 and *irt1* S206A lines under +Fe conditions.

Our histochemical detection of Fe in *irt1* roots using Perls stain located Fe accumulation predominantly in the cortex of the differentiation zone (Figure 2, Figure S7). We observed no Fe signal in cell walls in general. Transcript levels of a number of Fe status marker genes indicated an overall more sufficient Fe status in roots than in shoots of the *irt1* mutant, which can be taken to support that the Fe accumulated in roots of *irt1* is at least partly intracellular and physiologically accessible and sensed by the plant (Figures 7 and 8, Figures S8–S13). Our targeted search identified *BGLU45* as a possible marker transcript of local Fe status in root cortex cells that is in agreement with Fe levels in the *irt1* mutant (Figure S12), which will require dedicated confirmation in the future. The physiological Fe status of the shoots systemically governs the

transcriptional activation of a number of Fe deficiency-related genes in the roots (Giehl et al., 2012; Khan et al., 2018; Mendoza-Cózatl et al., 2014; Vert et al., 2003). This complicates the identification of cell type-specific markers of local Fe status in roots. In the *nramp1 irt1* double mutant Perls–DAB staining localized Fe in the walls of cortex cells, and the authors attributed this observation to the lack of *NRAMP1* function in the *irt1* genetic background (Castaings et al., 2016). The extensive sample preparation carried out in this study may have removed intracellularly localized Fe or deposited it onto cell walls.

When the high-affinity Fe²⁺ transporter IRT1 and/or the secondary Fe²⁺ transporter NRAMP1 are not present, endodermal suberization is delayed, which was proposed to facilitate the movement of Fe into the stele upon the entry into roots via the apoplastic or transcellular pathways (Barberon et al., 2016). Despite the decreased suberization and thus a generally increased permeability for ions into the stele in *irt1*, root-to-shoot Fe translocation is decreased and Fe accumulates in the cortex and endodermis of the *irt1* mutant (Figures 1 and 2), i.e., partly outward from the endodermis. Our results are consistent with the hypothesis that the inward transport of Fe²⁺ across the plasma membrane of root epidermal cells is not the only function of the IRT1 protein.

Phenotypic rescue of the root-to-shoot Fe partitioning defect of *irt1* by the transport-inactive mutant IRT1_{S206A} variant, but not of the Fe uptake defect of *irt1*

In addition to the well-known direct membrane transporter function of IRT1 in mediating the uptake of Fe²⁺ into root cells, we hypothesized that the IRT1 protein acts indirectly to de-repress root-to-shoot partitioning of Fe, based on the results presented here (Figure 1, Figures S1 and S2). If our hypothesis is correct, we would expect to observe the partial complementation of *irt1* mutant phenotypes by an IRT1 variant that is incapable of transporting Fe²⁺ but maintains indirect functionality. While the latter is entirely unknown to date, the direct transmembrane ion transport function of IRT1 is very well studied. Amino acid residues serine 206 and histidine 232 are both critical for the cellular import of Fe²⁺ (Figure 4, Figure S3), as well as that of secondary substrates Zn²⁺, Mn²⁺ and likely also Cd²⁺, conferred by IRT1 in the heterologous system *S. cerevisiae* (Eide et al., 1996; Rogers et al., 2000). While these earlier results are the basis of the *in planta* approach conducted here, transport properties observed in a heterologous system are not necessarily identical to *in planta* transport properties of a protein, which must be examined in the homologous system.

We introduced WT IRT1, IRT1_{S206A} and IRT1_{H232A} into an *irt1* mutant background and then tested for the rescue of various aspects of the phenotype of Arabidopsis *irt1* mutants. Our results are in agreement with our hypothesis, and they indicate that IRT1_{S206A} is inactive with respect to

the direct transmembrane Fe transport function of IRT1, but this variant protein maintains the indirect function at least partially. Our results suggest that, by contrast, IRT1_{H232A} is produced and stable *in planta*, but maintains neither the direct nor the indirect function of IRT1. We came to these conclusions by quantifying Fe concentrations and Fe deficiency symptoms in roots and shoots of seedlings (Figures 3–7, Figures S4–S11). Important support came from the quantification of Mn concentrations in tissues, exploiting the known transport activity of IRT1 for the secondary substrate Mn²⁺ in combination with IRT1 protein abundance under deficient and replete physiological Fe status (Figures 3, 5, and 6, Figure S4; Vert et al., 2002). Considering in combination root IRT1 protein levels and root Mn concentrations in *irt1* S206A lines in both +Fe and –Fe conditions suggested against residual transport activity for the secondary substrate Mn²⁺, and by extrapolation also for the primary substrate Fe²⁺, of IRT1_{S206A} *in planta* (see Results; Figures 3 and 6). Yet, we cannot fully exclude the possibility that the phenotypic complementation of *irt1* may rely on a small residual Fe²⁺ transport activity of IRT1_{S206A}, or another property of this protein variant that directly causes the observed phenotypic changes alone.

Intriguingly, we were unable to identify any difference between WT and *irt1* roots in short-term Fe accumulation, i.e., after 15 min of exposure to 2 μM radiolabeled Fe²⁺ (Figure 4(b), Table S2). Previous evidence from short-term Fe uptake assays *in planta* is scarce. In contrast to 2-week-old Fe-deficient WT plants, the *irt1* mutant (Ws background) was incapable of accumulating ⁵⁵Fe in shoots after 48 h (Vert et al., 2002). WT roots contained approximately 50% and *irt1-3* roots 70% of the total Fe accumulated per plant upon 1 h of pulse labeling with 3 μM ⁵⁹Fe-labeled Fe²⁺ *via* the roots of 2-week-old seedlings cultivated in Fe- and Zn-deficient medium. There was large quantitative variation and total Fe uptake averaged 130 ± 60 and 80 ± 30 fmol Fe plant⁻¹ in WT and *irt1-3*, respectively, and images suggested an overall smaller size of *irt1-3* than of WT seedlings used in the pulse labeling experiments (Henriques et al., 2002; T-DNA insertion 133 bp upstream of translational start codon). Although a direct or quantitative comparison with these two earlier studies is impossible, our results are in general agreement. Taking these studies together, the unequivocal defect in *irt1* mutants is a dramatically reduced Fe accumulation rate in shoots, whereas the root Fe accumulation rate in *irt1* is unchanged or even slightly enhanced. Thus, *irt1* mutants retain some root Fe uptake capacity independent of the IRT1 protein, suggesting that secondary Fe uptake systems operate in these mutants under the experimental conditions employed. An involvement of NRAMP1, for example, is possible, as proposed (Cailliatte et al., 2010; Castaings et al., 2016).

Secondary root Fe uptake systems are unable to fully compensate for the lack of IRT1 function under either –Fe

or +Fe cultivation conditions, based on the visible phenotypes and strongly lowered shoot Fe concentrations of *irt1* mutants (Figure 1 and Figure S2). Consistent with detectable levels of *IRT1* transcript and of IRT1 protein in roots of WT seedlings also upon cultivation in +Fe media (Figure 3 (a)), this suggests a biological relevance of IRT1 functions under both conditions. Compared to the WT, lowered total Fe levels per plant in *irt1* mutants are consistent with IRT1 contributing to root Fe uptake under both +Fe and –Fe conditions (Figure 6(c,d), Figures 1 and 2). The functioning of IRT1 in root Fe uptake under both cultivation conditions is supported by substantially higher root concentrations of Mn, a known secondary substrate of IRT1, in WT than in *irt1* also upon cultivation in +Fe medium (Figure 6(e,f)). According to our results, IRT1_{S206A} is transport-inactive (Figures 4(a), 5(e,f) and 6(e,f)) and thus only possesses the secondary function of IRT1 in root-to-shoot Fe partitioning identified here. Thus, in *irt1* S206A lines we do not expect to observe a full phenotypic rescue of the *irt1* mutant under either +Fe and –Fe conditions, in accordance with our results (Figures 3, 5 and 6, Figures S4 and S5).

Candidate genes for a role in IRT1-dependent Fe partitioning from the root to the shoot

It should be noted that our data do not support globally de-regulated Fe deficiency responses in relation to tissue Fe concentrations in *irt1* (Figure 8, Figures S8, S9, and S13). By contrast, Fe deficiency responses are constitutively activated in roots of *opt3-2* mutants and *IMA* overexpressor lines even when shoots contain excess levels of Fe (Grillet et al., 2018; Khan et al., 2018). Thus, the well-known systemic signaling of shoot Fe status to the root (Vert et al., 2003), which requires OPT3 and IMA peptides, is a process that is distinct from the IRT1 dependence of root-to-shoot Fe partitioning described here.

Our results support the hypothesis of a secondary function of IRT1 in the partitioning of Fe from the root to the shoot, which is at least partially independent of the primary function of IRT1 transmembrane Fe transport. Such a secondary function of IRT1 could involve a regulatory physical interaction of IRT1 with an unknown protein, which then triggers a process that finally results in the radial passage of Fe from root cortex cells inwards until Fe reaches the xylem, for example. Transceptor functions are known for several plant membrane transporters, for example NRT1.1 (Ho et al., 2009; Krouk et al., 2010) and also IRT1 (Dubeaux et al., 2018), in functional contexts differing from the one identified here. According to a symplastic pathway model, this IRT1-dependent process could encompass maintaining symplastic mobility of Fe through its chelation in the cytosol, suppressing the immobilization of Fe in vacuoles of root cortex cells, or fostering symplastic radial cell-to-cell passage of Fe *via* plasmodesmata. In a transcellular pathway model, the envisaged process could

involve cellular Fe efflux from root cortex cells and Fe re-uptake by endodermal cells. Proteins mediating any of these processes in a localized fashion remain unidentified. Finally, the presence of IRT1 could indirectly promote Fe export into the xylem vessels. IRT1-dependent de-repression of root-to-shoot partitioning may occur entirely through translational or post-translational regulation, or it may involve changes in transcript levels of some of the involved genes. Here we searched for candidate Fe deficiency-responsive transcripts that were under-responsive or non-responsive in roots of the *irt1* mutant.

By comparison to Fe-deficient WT, in roots of *irt1* we observed lower expression of several FIT-dependent (e.g., *CYP71B5*, *BGLU42*) and FIT-independent (e.g., *NAS4*, *bHLH101*) genes, among others (Table 1; Data S1 and S3; Bauer et al., 2007; Colangelo and Guerinot, 2004; Schwarz and Bauer, 2020; Zamioudis et al., 2015). Notably, the Fe deficiency-responsive increase in *MYB10* and *MYB72* transcript levels was strongly attenuated in *irt1* (Figure 8, Table 1). Root-specific transcription factors *MYB72* and *MYB10* regulate Fe partitioning to the shoot *via* activating *NAS4* transcription and thus NA biosynthesis in the stele (Palmer et al., 2013). Later, *MYB72* was found to also activate the transcription of genes encoding the enzymes *F6'H1* and *BGLU42* of the coumarin biosynthesis pathway that contribute to Fe mobilization in soil (Schmid et al., 2014; Stringlis et al., 2018; Zamioudis et al., 2014). In summary, decreased transcript levels of candidate genes *MYB72* and *MYB10*, and indirectly *NAS4*, may well account for impaired root-to-shoot partitioning of Fe in *irt1*. However, for these and a number of other potential candidate genes (Data S1–S4), we were unable to fully resolve whether their de-regulation is the cause or the effect of Fe immobilization in *irt1* roots.

In conclusion, here we provide evidence for a secondary, likely indirect and regulatory function of IRT1 in the partitioning of Fe from the root to the shoot. The ability of a transport-inactive *IRT1_{S206A}* variant to partially complement the *irt1* mutant supports our hypothesis and indicates that the secondary function of IRT1 is at least partly independent of its primary function of high-affinity Fe uptake into root epidermal cells. We identify previously characterized genes as candidate downstream targets of IRT1-dependent transcriptional regulation, which could contribute to Fe mobilization towards the shoot. Future work will be directed at the signaling and mechanisms of IRT1-dependent Fe partitioning from roots to shoots.

EXPERIMENTAL PROCEDURES

Plant material and growth conditions

Seeds of Col-0 were obtained from NASC. The *irt1-2* mutant (*pam42*, Col-0 background) was from Varotto et al. (2002). Ws and *irt1-1* seeds were kindly provided by Gregory Vert (CNRS/

University of Toulouse, Auzeville Tolosane, France). The transgenic lines *irt1 IRT1_P::IRT1* (WT *IRT1*), *irt1 IRT1_P::IRT1S206A* (*irt1 S206A*) and *irt1 IRT1_P::IRT1H232A* (*irt1 H232A*) were generated herein.

For sterile growth, seeds were washed in 70% (v/v) ethanol for 1 min, surface-sterilized with 1.4% (w/v) NaOCl and 0.02% (v/v) Triton X-100 for 10 min and washed five times with ultrapure water (Milli-Q; Merck). Following seed stratification at 4°C for 2 days, seedlings were pre-cultivated on a modified Hoagland's solution containing macro- and micronutrients as used in Haydon et al. (2012), supplemented with 1% (w/v) sucrose and solidified with 0.8% (w/v) agar Type M (Merck KGaA, Darmstadt, Germany). Ten-day-old seedlings were then transferred using titanium tweezers to modified Hoagland's solution supplemented with 1% (w/v) sucrose in which Fe was omitted from the nutrient solutions (–Fe treatment) or supplied as 10 μM FeHBED (+Fe treatment). Treatment media were solidified with 0.8% (w/v) agar Type M (Sigma) depleted from contaminant metals by EDTA-washing as described in Haydon et al. (2012). Seedlings were grown on vertically oriented square 120-mm polystyrene Petri dishes (Greiner Bio-One GmbH, Frickenhausen, Germany) in 11-h light (22°C, 145 μmol m⁻² sec⁻¹ white light) and 13-h dark (18°C) cycles (Percival CU-41L4; CLF Climatics). For selection of homozygous transgenic lines carrying a single T-DNA insertion, seeds were grown on 0.5× Murashige & Skoog (MS) medium (Duchefa Biochemie, Haarlem, The Netherlands) supplemented with 1% (w/v) sucrose, 0.8% (w/v) agar and hygromycin (30 μg ml⁻¹). In the T2 generation, five to six independent lines per construct were grown on MM media (Haydon and Cobbett, 2007) containing 1% (w/v) sucrose and 0.8% (w/v) agar Type M supplemented with hygromycin (30 μg ml⁻¹) for 10 days and then transferred to treatment media (+Fe treatment, as described above) for an additional 17 days before harvest (see Table S1). For hydroponic plant cultivation for short-term uptake assays of radiolabeled Fe, seeds were surface-sterilized, sown on 0.5× modified Hoagland's solution supplemented with 5 μM FeHBED (WT and *irt1 IRT1*) or 10 μM FeHBED (*irt1*, *irt1 S206A* and *irt1 H232A*) and solidified with 0.65% (w/v) Noble agar (Merck) in 0.7-ml black Eppendorf tubes and stratified at 4°C for 4 days. At the age of 7 days, the bottom third of each tube was cut off and about 60 tubes per line (1 seedling per tube) were transferred to a styrofoam tray floating on 4 L of 0.5× modified Hoagland's solution supplemented with 10 μM FeHBED (WT and *irt1 IRT1*) or 50 μM FeHBED (*irt1*, *irt1 S206A* and *irt1 H232A*) in a box covered with Saran wrap. After 1 week, plants were carefully transferred to smaller boxes (four plants per box in 420 ml solution, keeping roots separate per plant) containing modified Hoagland's solution supplemented with FeHBED as mentioned above (pre-cultivation). Plants were grown for an additional 5 weeks (WT and *irt1 IRT1*) to 6 weeks (*irt1*, *irt1 S206A* and *irt1 H232A*) with a weekly exchange of solutions to obtain vegetative stage plants of similar sizes. Roots were subsequently washed in 10 μM EDTA for 2 min and transferred into modified Hoagland's solution lacking FeHBED for 6 days (Fe deficiency treatment). Plants were grown in 11-h light (20°C, 145 μmol m⁻² sec⁻¹ white light) and 13-h dark (18°C) cycles (Percival CU-41L4; CLF Climatics) in a tray that was covered with a transparent cover, which was removed during the final 3 weeks of cultivation. For the confirmation experiment at MU, pre-cultivation was in 5 μM (WT) and 50 μM FeHBED (*irt1*) for 4 to 5 weeks, and Fe deficiency treatment was in 0 μM (WT) and 5 μM (*irt1*) FeHBED for 5 days. For soil cultivation, seeds were germinated on Minitray soil (Balster Einheitserdewerk, Fröndenberg) after 4 days of stratification at 4°C. Plants were grown under the same environmental conditions as for sterile growth for 3 weeks.

Yeast constructs, strains and growth

The *IRT1* coding cDNA sequence, including the translational start and stop codons, was amplified from the corresponding transgenic plant line by RT-PCR with IRT1-ATG_F 5'-CACCAT GGCTCAAATTCAGCAC-3' and IRT1-cDNA_TAA_R 5'-TTAAGCCC ATTTGGCGATAATCG-3', introduced into pENTR-D/TOPO (Invitrogen, Carlsbad, CA, USA) and cloned into the yeast expression vector pFL61-Gateway (Desbrosses-Fonrouge et al., 2005) using LR clonase (Invitrogen) according to the manufacturer's protocol. Mutations S206A and H232A were introduced by a modified Quik-Change protocol (Zheng et al., 2004) using KAPAHifi DNA polymerase (PEQLAB Biotechnology, Erlangen, Germany) and the primers AtIRT1_S198A_For 5'-TAGTTCACGCGTGGTCATTGGAT TATC-3', AtIRT1_S198A_Rev 5'-CCACCGCGTGAACATGATCCCAA G-3', AtIRT1_H224A_For 5'-TGCTTCGCTCAAATGTTGCAAGGCATG GG-3' and AtIRT1_H224A_Rev 5'-CATTTGAGCGAAGCAAAGAGC TGCTATAAGTC3'. All constructs were verified by Sanger sequencing. For complementation assays, competent *S. cerevisiae* yeast cells of WT (DY1457) and *fet3fet4* mutant (DEY1453; Dix et al., 1994) strains were transformed with each construct or the empty vector (Dohmen et al., 1991). As a positive control, the corresponding WT yeast strain was transformed with the empty vector. Transformants were selected on SD media lacking uracil (SD-Ura) pH 5.7, 2% (w/v) Bacto-Agar, with 2% (w/v) D-glucose as a carbon source. For each construct, three independent transformant colonies were grown overnight at 30°C in 2 ml liquid SD-Ura pH 3.5 with 2% (w/v) D-glucose supplemented with 10 µM FeCl₃, to early stationary phase (OD₆₀₀ ≈ 0.3, approximately 10⁷ cells ml⁻¹). Yeast cells were then centrifuged at 15 700 × g for 1 min, washed once in SD-Ura pH 5.7 with 2% (w/v) D-glucose to remove residual Fe and subsequently resuspended in the same medium. Aliquots of 10 µl of 10-fold serially diluted cell suspensions (OD₆₀₀ of 0.3, 0.03, ...) were spotted onto SD-Ura pH 5.7 containing 2% (w/v) Bacto-Agar and 2% (w/v) D-glucose, supplemented with 0.5 mM FeSO₄ or left unamended. Plates were incubated at 30°C for 3 days and photographed using a Nikon Digital SLR camera with an AF-S DX Zoom NIKKOR 18-70 mm 1:3,5-4,5G ED-IF objective.

Generation of transgenic plants

For genetic complementation of the *irt1* mutant with WT *IRT1*, the promoter region (1024 bp upstream of the translational start codon), the coding region, and the 3' untranslated region sequence (310 bp downstream of the stop codon) were amplified by PCR using Phusion DNA polymerase (NEB) from genomic Col-0 DNA with IRT1p_-1024F 5'-CACCGACACATTAAACATTCAT ACCCGATT-3' and IRT1_1546R 5'-CTTTAATTTACTTATCTTGGAAA AAGCAGC-3'. For the mutant variants *IRT1*_{S206A} and *IRT1*_{H232A}, overlapping PCR products were generated with IRT1p_-1024F and IRT1_S198A_R 5'-GATAATCCAATGACCACCGCGTGAACATGAT CCCAAG-3' or IRT1_H224A_R 5'-CCATGCCTTCGAACATTTGAGC GAAGCAAAGAGCTGC-3' and IRT1_1546R and IRT1_S198A_F 5'-CTTGGGATCATAGTTCACGCGTGGTCATTGGATTATC-3' or IRT1_H224A_F 5'-GCAGCTCTTGTTCGCTCAAATGTTGCAAGGCATGG-3'. These PCR products were combined in a subsequent PCR reaction using only IRT1_-1024F and IRT1_1546R to generate the full-length mutant variants. WT and mutant PCR products were introduced into pENTR-D/TOPO (Invitrogen) and verified by Sanger sequencing before recombining into a modified pMDC32 vector (Curtis and Grossniklaus, 2003) lacking the 35S promoter using LR Clonase (Invitrogen) (Hanikenne et al., 2008). Plasmids were introduced into *Agrobacterium tumefaciens* GV3101 by electroporation and transformed into *irt1* by floral dip (Clough and Bent, 1998).

Homozygous T3 seeds carrying single-locus insertions of two independent transgenic lines per construct were chosen for detailed characterization based on shoot Fe concentrations in the T2 generation (Table S1).

Microarray-based transcriptomics

All methods in this section are described according to MIAME recommendations. Fifteen-day-old seedlings were used for the microarray experiment. Roots and shoots were harvested separately at ZT 3 h, flash-frozen in liquid nitrogen and subsequently stored at -80°C. RNA was extracted using an RNeasy Plant Mini Kit with on-column DNase I digestion (Qiagen, Hilden, Germany). cRNA labeling and ATH1 hybridization were performed according to the manufacturer's instructions at GeneCore Facility, EMBL, Heidelberg. The array GeneChip ATH1-121501 (Thermo Fisher Scientific, former Affymetrix), which contains 22 500 probe sets representing approximately 24 000 gene sequences of the *A. thaliana* genome, was used for hybridizations. Replicate ATH1 arrays were hybridized with labeled cRNA from two independent experiments, with six samples per experiment: shoots or roots of WT +Fe, WT -Fe and *irt1* +Fe. Signal intensities were imported into Genespring (Version 8; Agilent Technologies, Santa Clara, CA, USA), and an RMA normalization was performed without transformation. Differentially expressed genes (DEGs) were selected by ≥ 2-fold difference in mean normalized signal in both replicates and an unpaired Mann-Whitney test with Benjamini-Hochberg adjustments for multiple comparisons, with a cutoff value of $P < 0.15$. The gene lists obtained with different comparisons were then intersected with one another to identify overlapping DEGs using Venn Selector at VIB (UGent; <http://bioinformatics.psb.ugent.be/webtools/Venn>).

RT-qPCR

For gene expression analysis using RT-qPCR, seedlings were grown and harvested as for the microarray experiments. Total RNA was extracted from 30 to 50 mg of frozen powdered tissue with TRIzol Reagent following the manufacturer's instructions. Total RNA was treated with 2 U of DNase per 10 µg of total RNA using the TURBO DNA-free™ Kit (Thermo Fisher Scientific, former Ambion). Integrity of DNA-free RNA was verified in Bleach Gel (Aranda et al., 2012), and the A₂₈₀/A₂₆₀ ratio in NanoDrop™ 2000/2000c (Thermo Fisher Scientific) was used to assess RNA quality. One microgram of DNase-treated RNA and oligo (dT)₁₈ primers were used in first-strand cDNA synthesis with the RevertAid First Strand cDNA Synthesis Kit (Thermo Fisher Scientific) following the manufacturer's instructions. RT-qPCR was performed on a LightCycler480 (Roche, Basel, Switzerland) in a 10-µl reaction mixture containing 8 ng of cDNA, each primer at 0.25 µM and 5 µl of 2 × GoTaq qPCR Master Mix (Promega, Madison, WI, USA). The amplification program consisted of pre-incubation steps at 50°C for 2 min and 95°C for 10 min followed by 40 cycles of 95°C for 15 sec and 60°C for 1 min. A final dissociation step of 95°C for 10 sec and 65°C for 5 sec was included for melting curve analysis. Reaction efficiencies (E) for each PCR reaction were determined with the LinRegPCR program, version 2016.0 (Ruijter et al., 2009) and used to calculate the transcript level as $TL = E^{-Ct}$, with Ct as the cycle threshold. Relative transcript levels (RTLs) were calculated by dividing the transcript level of the gene of interest by the geometric mean of transcript levels of two housekeeping genes, *UBQ10* and *EF1α*. All oligonucleotide sequences are specified in Table S3.

Ionomics and biomass estimates

Twenty-day-old seedlings were used for the quantification of metal concentrations. Shoots and roots were harvested separately

by cutting below the hypocotyl with a scalpel washed in 10 mM EDTA. Root and shoot tissues were pooled per plate and desorbed by washing in 5 mM CaSO₄, 10 mM MES-KOH, pH 5.7 for 10 min, in 5 mM CaSO₄, 10 mM Na₂EDTA, pH 5.7 for 5 min and twice in ultrapure water for 1 min, all carried out on ice with occasional stirring. After desorbing, tissue pools were blotted dry using paper towels (Blauer Engel), and fresh biomass (FW) was recorded and calculated per plant. Aliquots of 4–25 mg of powdered dry biomass per sample were digested as described in Sinclair et al. (2017). Multi-element analysis was conducted using Inductively Coupled Plasma Optical Emission Spectrometry (ICP-OES) in an iCAPDuo 6500 instrument (Thermo Fisher Scientific), following calibration with a blank and a series of five multi-element standards from single-element standard solutions (AAS Standards; Bernd Kraft). The precision of measurements was validated by measuring a sample blank and an intermediate calibration standard solution, as well as digests of a certified reference material (Virginia tobacco [*Nicotiana benthamiana*] leaves, INCT-PVTL 6; Institute of Nuclear Chemistry and Technology, PL) before and after every sample series. To ensure timely handling of the samples, we divided the panel of transgenic lines into two sets, each representing all constructs, and we used in each experiment one set plus WT and *irt1*.

Whole-mount staining of non-heme Fe with Perls reagent

Seven-day-old seedlings germinated and grown in standard media were harvested at ZT 1 h. Three seedlings were pooled in a 2-ml tube, washed once with ice-cold 10 mM EDTA pH 5.7 for 5 min and three times with ice-cold ultrapure water for 1–2 min. Seedlings were then submerged in 1 ml Perls solution (2% [v/v] HCl and 2% [w/v] potassium ferrocyanide), vacuum infiltrated for 15 min (500 mbar) and incubated at room temperature for 30 min (Roschztardt et al., 2009). Seedlings were then rinsed twice with ultrapure water and mounted in ultrapure water for visualization on an Imager.M2 (Zeiss, Oberkochen, Germany).

Chlorophyll and root length measurements

Quantification of leaf chlorophyll content and root length were done on 15-day-old seedlings. For chlorophyll measurements, 34–52 mg of pooled shoots (5–8 seedlings) were harvested into a 2-ml tube, flash-frozen in liquid nitrogen and homogenized with a plastic pestle cooled in liquid nitrogen. After the addition of 1.5 ml 100% (v/v) methanol (Merck), samples were covered with aluminum foil and incubated at 70°C for 15 min, with stirring at 850 rpm for 10 sec every 5 min. After cooling on ice for 5 min, methanol extracts were cleared by centrifugation at 16 000 × g, 4°C, for 1 min. Absorbance (extinction) values were measured at 652 nm and 665 nm in a Synergy HTX Multi-Mode Reader (Agilent, former BioTek, Santa Clara, CA, USA), using methanol as a blank. Microplate path length correction was applied according to Warren (2008). Chlorophyll concentrations were calculated following Porra et al. (1989). Three repeated measurements of each sample served as technical replicates. For root elongation estimates, the positions of primary root tips of 10-day-old seedlings were marked with a permanent marker (Edding[®] 400) on the bottom of the Petri plate immediately after transfer to +Fe or –Fe treatment media. Five days afterwards, seedlings were imaged with a Nikon Digital SLR camera with an AF-S DX Zoom NIKKOR 18–70 mm 1:3.5–4.5G ED-IF objective at 50 mm distance. Primary root length was measured using ImageJ (Schneider et al., 2012) by drawing a segmented line along the main root.

Root surface Ferric Chelate Reductase activity assays

Seedlings were grown as for microarray experiments. Roots of 5 to 8 15-day-old seedlings (8–33 mg fresh biomass) were harvested at ZT 3 h using a scalpel, pooled and immediately transferred to 2-ml tubes securely capped to avoid humidity loss. Roots were incubated in 1.5 ml of assay solution (0.1 mM Fe(III)EDTA, 0.3 mM FerroZine) at room temperature in darkness for 20 min (time course experiment) or 40 min (FCR activity after Fe deficiency for 5 days). After reading absorbance at 535 nm on a PowerWave XS2 plate reader (Agilent, former BioTek), Fe(II)FerroZine concentrations were calculated using an extinction coefficient of 28.6 mM⁻¹ cm⁻¹ (Gibbs, 1976).

IRT1 Immunoblots

Total protein was extracted from 30 mg FW of pooled root tissues as described earlier (Sgula et al., 2008) with the difference that 2% (w/v) DTT was used as reducing agent and that prior to centrifugation, protein extracts were incubated 5 min at room temperature to facilitate membrane solubilization. Total protein in the supernatants was quantified in 1:5 dilutions with the Pierce[™] BCA Protein Assay Kit using BSA as a standard. Per sample, 20 µg of total protein was mixed with ultrapure water and 2 µl of 6× loading buffer (375 mM Tris-HCl, pH 6.8, 30% [v/v] mercaptoethanol, 0.03% [v/v] bromophenol blue, 12% [w/v] SDS, and 60% [v/v] glycerol) in a final volume of 12 µl and subsequently incubated for 20 min at 37°C. Proteins were separated by 12% (w/v) SDS-PAGE and blotted onto a polyvinylidene difluoride (PVDF) membrane by wet/tank transfer (Towbin et al., 1979). The PVDF membrane was blocked with 5% (w/v) skim milk in TBS-T (0.05% Tween-20) at room temperature for 1 h and probed with anti-IRT1 antibody (generally 1:5000; in Figure S4(b), 1:1000; Agrisera AS111780, Lot number 1203) in 2.5% (w/v) skim milk in TBS-T (0.05% Tween-20) at room temperature for 1 h. Following incubation at room temperature for 1 h with horseradish peroxidase (HRP)-conjugated goat anti-rabbit IgG (H + L) (1:20 000, Thermo Fisher Scientific 31466; lot number RL243150) in 2.5% (w/v) skim milk in TBS-T, chemiluminescence signals were detected with ECL Select Western Blotting Detection Reagent (GE Healthcare) and a Fusion Fx7 documentation system (Vilber Lourmat) for 4 sec (except Figure S4(b): 30 sec).

Short-term uptake rates of ⁵⁵Fe

Hydroponically cultivated 7.5-week-old (WT and *irt1*) or 8.5-week-old (*irt1*, *irt1* S206A and *irt1* H232A) plants of equal sizes were used for short-term Fe uptake assays. To allow for accurate sample processing we included one line per construct, WT and *irt1* in each experiment. At ZT 1 h, the root systems of four to five replicate plants per line were submerged in glass liquid scintillation vials (one plant per vial) containing 35 ml of 1 mM MES-KOH pH 5.7, 2.1 µM citrate, 1 mM ascorbic acid and 2 µM ⁵⁵Fe (⁵⁵FeCl₃, 0.0197 MBq nmol⁻¹, Perkin-Elmer). After two incubations of 1.5 min and 15 min duration for each genotype, respectively, roots were desorbed by washing three times in fresh ice-cold solution of 5 mM CaSO₄, 10 mM Na₂EDTA pH 5.7, 1 mM MES-KOH pH 5.7 for 5 min (40 ml per plant). Roots were cut off, carefully blotted dry between paper towels (Blauer Engel), weighed and stored at –20°C for 24 h in 6-ml HPDE scintillation vials to destroy the cells. Roots were then suspended in 4 ml of scintillation cocktail at room temperature (Rotiszint, Carl Roth, Germany). Counting was performed twice for each sample (10 min per sample) with a β-scintillation counter Beckman LS6000TA (Beckman Coulter, USA). Roots of two plants identically grown and processed but

not exposed to the incubation solution were used to determine background counts. For calculation of ^{55}Fe uptake, values of uptake after 1.5 min were subtracted from those after 15 min uptake and expressed as $\text{nmol } ^{55}\text{Fe g}^{-1} \text{FW h}^{-1}$. Pre-cultivation periods and conditions varied slightly from experiment to experiment, gradually obtaining plants of more and more equivalent sizes and developmental stages for all genotypes. For a confirmation experiment at MU (Table S2), plants of similar size grown hydroponically were pre-incubated in 35 ml of a solution of 0.2 mM CaSO_4 , 1 mM ascorbic acid, 5 mM MES-TRIS, pH 5.0 for 30 min and then transferred to 30 ml of uptake buffer of identical composition with the addition of 1 μM FeCl_3 (spiked with approximately 2 $\mu\text{Ci } ^{59}\text{Fe}$) for an uptake period of 120 min. Washing solutions were composed as follows: 20 mM TRIS, 5 mM EDTA (30 ml for 10 min, followed by 35 ml for 10 min), ultrapure water (25 ml for 5 min, twice). Roots were separated from shoots and blotted dry as described above before scintillation counting. Vials containing only scintillation cocktail were used for background subtraction.

Statistical analysis

Statistical analyses were conducted in R Studio Version 1.1.456 (R Core Team, 2020). Two-factor analysis of variance (ANOVA) was performed assuming the following linear model: $\text{model} = \text{lm}(\text{Var1} \sim + \text{GENOTYPE} + \text{TREATMENT}:\text{GENOTYPE})$. Tukey's honestly significant difference (HSD) test was applied in multiple comparisons of means. Alternatively, when homoscedasticity was not met ($P < 0.05$, Levene's test), pairwise Welch *t*-tests were conducted. When normality was not met ($P < 0.05$, Shapiro-Wilk test), pairwise Student's *t*-tests were used. For all *t*-tests, pairwise differences were considered significant when false discovery rate-corrected $q < 0.05$.

ACCESSION NUMBERS

Sequence data for the genes mentioned in the text can be found on The Arabidopsis Information Resource (TAIR) or the GenBank website. Accession numbers are (in alphabetical order): *ALTERNATIVE OXIDASE1A (AOX1A)*, AT3G22370; *basic HELIX LOOP HELIX39 (bHLH39)*, AT3G56980; *basic HELIX LOOP HELIX 101 (bHLH101)*, AT5G04150; *BETA-GLUCOSIDASE42 (BGLU42)*, AT5G36890; *BETA-GLUCOSIDASE45 (BGLU45)*, AT1G61810; *BRUTUS-LIKE2 (BTSL2)*, AT1G18910; *CYTOCHROME P45071b5 (CYP71B5)*, AT3G53280; *DETOXIFICATION1 (DTX1)*, AT2G04040; *FERRITIN1 (FER1)*, AT5G01600; *IRONMAN1 (IMA1)*, AT1G47400; *IRON-REGULATED TRANSPORTER1 (IRT1)*, AT4G19690; *IRON-REGULATED TRANSPORTER2 (IRT2)*, AT4G19680; *MYB DOMAIN PROTEIN10 (MYB10)*, AT3G12820; *MYB DOMAIN PROTEIN 72 (MYB72)*, AT1G56160; *NICOTIANAMINE SYNTHASE4 (NAS4)*, AT1G56430; *ZRT/IRT-LIKE PROTEIN 2 (ZIP2)*, AT5G59520; *ZINC-INDUCED FACILITATOR1 (ZIF1)*, AT5G13740.

ACKNOWLEDGMENTS

The *fet3fet4* and corresponding WT yeast strains were kindly provided by Prof. Dr. David Eide (University of Wisconsin-Madison, US), and the Arabidopsis *pam42* mutant was generously provided by Prof. Dr. Dario Leister (LM University Munich, Germany). We are grateful to Petra DÜchting for multi-element analysis, Dr. Lara Syllwasschy for *t*-test scripts, Andreas Aufermann and Iris Sandorf

for technical assistance in plant cultivation and all lab members for comments (Ruhr University Bochum, Germany). We also thank M.A. Luján and P. Lorente for technical support and R. Picorel for providing infrastructure (EEAD, CSIC, Spain). This work was supported by Deutsche Forschungsgemeinschaft grants Kr1967/3-3 and 15-1, European Union FOOD-CT-2006-016253 and ERC-AdG LEAP EXTREME (788380) to UK, Ruhr University Bochum, European Union fellowship PIIF-GA-2008-219457 to MJH and Araid-Ibercaja-young scientist grant 2010, as well as Juan de la Cierva (MICINN) and JAE-DOC (CSIC) funding, to MB. Open Access funding enabled and organized by Projekt DEAL.

CONFLICT OF INTEREST

The authors declare no conflict of interest.

AUTHOR CONTRIBUTIONS

MJH, MB and UK conceived the project; MJH, MB, JQ and UK designed research; JQ, MS, MB, MJH, HH-C and MP performed experiments; JQ, MB, MJH and UK analyzed data; NN and DM-C confirmed independently the short-term Fe uptake; and JQ and UK wrote the manuscript, with contributions from MB, MS, MJH and HH-C. All authors read and edited the manuscript.

SUPPORTING INFORMATION

Additional Supporting Information may be found in the online version of this article.

Figure S1. Details of the *irt1* phenotype.

Figure S2. The *irt1-1* mutant in the Ws background overaccumulates Fe in the root.

Figure S3. Topology model of IRT1 highlighting the amino acid residues mutated in this paper.

Figure S4. Details of *IRT1* expression in transport-inactive mutants.

Figure S5. Photographs of Arabidopsis WT, *irt1*, *irt1* IRT1, *irt1* S206A and *irt1* H232A plants.

Figure S6. Root and shoot Zn and Cu concentrations.

Figure S7. Rescue of Fe accumulation in sub-epidermal cell layers of *irt1* S206A roots.

Figure S8. Fe deficiency responses are not constitutively activated in shoots of *irt1* S206A lines.

Figure S9. Experimental rationale of transcriptomic analysis.

Figure S10. Heatmap of candidate genes for roles in IRT1-dependent root-to-shoot Fe partitioning.

Figure S11. Validation of microarray data using RT-qPCR.

Figure S12. Lack of Fe deficiency response in cortex-enriched transcripts in the *irt1* mutant.

Figure S13. Transcript levels of candidate genes for roles in IRT1-dependent root-to-shoot translocation across genotypes.

Table S1. Fe concentrations in shoots of independent transgenic lines for *irt1* IRT1, *irt1* S206A and *irt1* H232A.

Table S2. Short-term uptake of radiolabeled Fe into roots of Fe-deficient wild-type and *irt1* mutant plants.

Table S3. Oligonucleotides used in the present study.

Data S1. List of overlapping differentially expressed genes between $-\text{Fe}$ versus C (WT) and *irt1* (C) versus WT ($-\text{Fe}$) in roots (**, *; Figure 8(a,b)).

Data S2. List of differentially expressed genes that overlap between –Fe versus C (WT) and *irt1* versus WT (C) in roots (#; Figure 8(a,b)).


Data S3. List of overlapping differentially expressed genes between –Fe versus C (WT) and *irt1* (C) versus WT (-Fe) in shoots (**, *; Figure 8(c,d)).

Data S4. List of differentially expressed genes that overlap between –Fe versus C (WT) and *irt1* versus WT (C) in shoots (#; Figure 8(c,d)).

Data S5. List of transcripts reported at higher or lower abundance in the stele versus the cortex that were Fe deficiency-responsive according to this study.

Data S6. List of transcripts reported at higher or lower abundance in the stele versus the endodermis that were Fe deficiency-responsive according to this study.

OPEN RESEARCH BADGES

 This article has earned an Open Data badge for making publicly available the digitally shareable data necessary to reproduce the reported results. The data are available at <https://www.ncbi.nlm.nih.gov/geo/query/acc.cgi?acc=GSE166269>.

DATA AVAILABILITY STATEMENT

The microarray data set (GSE166269) is available at <https://www.ncbi.nlm.nih.gov/geo/query/acc.cgi?acc=GSE166269>.

All other relevant data can be found within the manuscript and its supporting materials. To obtain materials or other raw data generated in this study please contact the corresponding author.

REFERENCES

- Alberts, B., Johnson, A., Lewis, J., Raff, M., Roberts, K., Walter, P. *et al.* (2002) *The evolution of electron-transport chains in molecular biology of the cell*, 4th edition. New York: Garland Science Available from: <https://www.ncbi.nlm.nih.gov/books/NBK26849/>
- Aranda, P.S., LaJoie, D.M. & Jorcyk, C.L. (2012) Bleach gel: a simple agarose gel for analyzing RNA quality. *Electrophoresis*, **33**, 366–369.
- Barberon, M., Dubeaux, G., Kolb, C., Isono, E., Zelazny, E. & Vert, G. (2014) Polarization of IRON-REGULATED TRANSPORTER1 (IRT1) to the plant-soil interface plays crucial role in metal homeostasis. *Proceedings of the National Academy of Sciences of the United States of America*, **111**, 8293–8298.
- Barberon, M., Vermeer, J., De Bellis, D., Wang, P., Naseer, S., Andersen, T. *et al.* (2016) Adaptation of root function by nutrient-induced plasticity of endodermal differentiation. *Cell*, **164**, 447–459.
- Barberon, M., Zelazny, E., Robert, S., Conéjéro, G., Curie, C., Friml, J. *et al.* (2011) Monoubiquitin-dependent endocytosis of the IRON-REGULATED TRANSPORTER1 (IRT1) transporter controls iron uptake in plants. *Proceedings of the National Academy of Sciences of the United States of America*, **108**, E450–E458.
- Bauer, P., Ling, H.-Q. & Guerinot, M. (2007) FIT, the FER-like iron deficiency induced transcription factor in Arabidopsis. *Plant Physiology and Biochemistry*, **45**, 260–261.
- Bauer, P., Thiel, T., Klatte, M., Berezcky, Z., Brumbarova, T., Hell, R. *et al.* (2004) Analysis of sequence, map position, and gene expression reveals conserved essential genes for iron uptake in Arabidopsis and tomato. *Plant Physiology*, **136**, 4169–4183.
- Baxter, I.R., Vitek, O., Lahner, B., Muthukumar, B., Borghi, M., Morrissey, J. *et al.* (2008) The leaf ionome as a multivariable system to detect a plant's physiological status. *Proceedings of the National Academy of Sciences of the United States of America*, **105**, E12081–E12086.
- Becher, M., Talke, I.N., Krall, L. & Krämer, U. (2004) Cross-species microarray transcript profiling reveals high constitutive expression of metal

homeostasis genes in shoots of the zinc hyperaccumulator *Arabidopsis halleri*. *The Plant Journal*, **37**, 251–268.

- Brady, S.M., Orlando, D.A., Lee, J.-Y., Wang, J.Y., Koch, J., Dinneny, J.R. *et al.* (2007) A high-resolution root spatiotemporal map reveals dominant expression patterns. *Science*, **318**, 801–806.
- Briat, J.-F., Duc, C., Ravet, K. & Gaymard, F. (2009) Ferritins and iron storage in plants. *Biochimica Et Biophysica Acta*, **1800**, 806–814.
- Buckhout, T.J., Yang, T.J.W. & Schmidt, W. (2009) Early iron-deficiency-induced transcriptional changes in Arabidopsis roots as revealed by microarray analyses. *BMC Genomics*, **10**, 147.
- Cailliatte, R., Schikora, A., Briat, J.-F., Mari, S. & Curie, C. (2010) High-affinity manganese uptake by the metal transporter NRAMP1 is essential for Arabidopsis growth in low manganese conditions. *The Plant Cell*, **22**, 904–917.
- Castaigns, L., Caquot, A., Loubet, S. & Curie, C. (2016) The high-affinity metal transporters NRAMP1 and IRT1 team up to take up iron under sufficient metal provision. *Scientific Reports*, **6**, 37222.
- Chaney, R.L. (1988) Plants can utilize iron form Fe-N, N'-di-(2-hydroxybenzoyl)-ethylenediamine-N, N'-diacetic acid, a ferric chelate with 106 greater formation constant than Fe-EDDHA. *Journal of Plant Nutrition*, **11**, 1033–1050.
- Chapelle, A., Morreel, K., Vanholme, R., Le-Bris, P., Morin, H., Lapierre, C. *et al.* (2012) Impact of the absence of stem-specific β -Glucosidases on lignin and monolignols. *Plant Physiology*, **160**, 1204–1217.
- Clough, S.J. & Bent, A.F. (1998) Floral dip: a simplified method for Agrobacterium-mediated transformation of Arabidopsis thaliana. *The Plant Journal*, **16**, 735–743.
- Colangelo, E.P. & Guerinot, M.L. (2004) The Essential Basic Helix-Loop-Helix Protein FIT1 is required for the iron deficiency response. *The Plant Cell*, **16**, 3400–3412.
- Connolly, E.L., Campbell, N.H., Grotz, N., Prichard, C.L. & Guerinot, M. (2003) Overexpression of the FRO2 Ferric Chelate Reductase confers tolerance to growth on low iron and uncovers posttranscriptional control. *Plant Physiology*, **133**, 1102–1110.
- Connolly, E.L., Fett, J.P. & Guerinot, M.L. (2002) Expression of the IRT1 metal transporter is controlled by metals at the levels of transcript and protein accumulation. *The Plant Cell*, **14**, 1347–1357.
- Curtis, M.D. & Grossniklaus, U. (2003) A gateway cloning vector set for high-throughput functional analysis of genes in planta. *Plant Physiology*, **133**, 462–469.
- Desbrosses-Fonrouge, A.-G., Voigt, K., Schröder, A., Arrivault, S., Thomine, S. & Krämer, U. (2005) Arabidopsis thaliana MTP1 is a Zn transporter in the vacuolar membrane which mediates Zn detoxification and drives leaf Zn accumulation. *FEBS Letters*, **579**, 4165–4174.
- Dinneny, J.R., Long, T.A., Wang, J.Y., Jung, J.W., Mace, D., Pointer, S. *et al.* (2008) Cell identity mediates the response of Arabidopsis roots to abiotic stress. *Science*, **320**, 942–945.
- Dix, D.R., Bridgham, J.T., Broderius, M.A., Byersdorfer, C.A. & Eide, D.J. (1994) The *FET4* gene encodes the low affinity Fe(II) transport protein of *Saccharomyces cerevisiae*. *Journal of Biological Chemistry*, **269**, 26092–26099.
- Dohmen, R.J., Strasser, A.W.M., Höner, C.B. & Hollenberg, C.P. (1991) An efficient transformation procedure enabling long-term storage of competent cells of various yeast genera. *Yeast*, **7**, 691–692.
- Dubeaux, G., Neveu, J., Zelazny, E. & Vert, G. (2018) Metal Sensing by the IRT1 transporter-receptor orchestrates its own degradation and plant metal nutrition. *Molecular Cell*, **69**, 953–964.e5.
- Eide, D., Broderius, M., Fett, J. & Guerinot, M.L. (1996) A novel iron-regulated metal transporter from plants identified by functional expression in yeast. *Proceedings of the National Academy of Sciences of the United States of America*, **93**, 5624–5628.
- Gao, F., Robe, K., Bettembourg, M., Navarro, N., Rofidal, V., Santoni, V. *et al.* (2020a) The Transcription Factor bHLH121 interacts with bHLH105 (ILLR3) and its closest homologs to regulate iron homeostasis in Arabidopsis. *The Plant Cell*, **32**, 508.
- Gao, F., Robe, K. & Dubos, C. (2020b) Further insights into the role of bHLH121 in the regulation of iron homeostasis in *Arabidopsis thaliana*. *Plant Signaling and Behavior*, **15**, 1795582.
- Gibbs, C.R. (1976) Characterization and application of FerroZine iron reagent as a ferrous iron indicator. *Analytical Chemistry*, **48**, 1197–1201.

- Giehl, R., Lima, J.E. & von Wirén, N. (2012) Localized iron supply triggers lateral root elongation in Arabidopsis by altering the AUX1-mediated auxin distribution. *The Plant Cell*, **24**, 33–49.
- Gollhofer, J., Timofeev, R., Lan, P., Schmidt, W. & Buckhout, T.J. (2014) Vacuolar-iron-transporter1-like proteins mediate iron homeostasis in Arabidopsis. *PLoS One*, **9**, e110468.
- Green, L.S. & Rogers, E.E. (2004) FRD3 Controls iron localization in Arabidopsis. *Plant Physiology*, **136**, 2523–2531.
- Grillet, L., Lan, P., Li, W., Mokkupati, G. & Schmidt, W. (2018) IRON MAN is a ubiquitous family of peptides that control iron transport in plants. *Nature Plants*, **4**, 953–963.
- Hanikenne, M., Talke, I.N., Haydon, M., Lanz, C., Nolte, A., Motte, P. et al. (2008) Evolution of metal hyperaccumulation required cis-regulatory changes and copy number expansion of *HMA4*. *Nature*, **453**, 391–394.
- Haydon, M.J. & Cobbett, C.S. (2007) A novel major facilitator superfamily protein at the tonoplast influences zinc tolerance and accumulation in Arabidopsis. *Plant Physiology*, **143**, 1705–1719.
- Haydon, M.J., Kawachi, M., Wirtz, M., Hillmer, S., Hell, R. & Krämer, U. (2012) Vacuolar nicotianamine has critical and distinct roles under iron deficiency and for zinc sequestration in Arabidopsis. *The Plant Cell*, **24**, 724–737.
- Henriques, R., Jásik, J., Klein, M., Martinoia, E., Feller, U., Schell, J. et al. (2002) Knock-out of Arabidopsis metal transporter gene IRT1 results in iron deficiency accompanied by cell differentiation defects. *Plant Molecular Biology*, **50**, 587–597.
- Ho, C.H., Lin, S.H., Hu, H.C. & Tsay, Y.F. (2009) CHL1 functions as a nitrate sensor in plants. *Cell*, **138**(6), 1184–94.
- Ivanov, R., Brumbarova, T., Blum, A., Jantke, A.M., Fink-Straube, C. & Bauer, P. (2014) SORTING NEXIN1 is required for modulating the trafficking and stability of the Arabidopsis IRON-REGULATED TRANSPORTER1. *The Plant Cell*, **26**, 1294–1307.
- Jakoby, M., Wang, H.-Y., Reidt, W., Weisshaar, B. & Bauer, P. (2004) FRU (BHLH029) is required for induction of iron mobilization genes in *Arabidopsis thaliana*. *FEBS Letters*, **577**, 528–534.
- Kerkeb, L., Mukherjee, I., Chatterjee, I., Lahner, B., Salt, D.E. & Connolly, E.L. (2008) Iron-induced turnover of the Arabidopsis IRON-REGULATED TRANSPORTER1 metal transporter requires lysine residues. *Plant Physiology*, **146**, 1964–1973.
- Khan, M.A., Castro-Guerrero, N.A., McInturf, S.A., Nguyen, N.T., Dame, A.N., Wang, J. et al. (2018) Changes in iron availability in Arabidopsis are rapidly sensed in the leaf vasculature and impaired sensing leads to opposite transcriptional programs in leaves and roots. *Plant, Cell and Environment*, **41**, 2263–2276.
- Kim, S.A., LaCroix, I.S., Gerber, S.A. & Guerinot, M. (2019) The iron deficiency response in *Arabidopsis thaliana* requires the phosphorylated transcription factor URI. *Proceedings of the National Academy of Sciences of the United States of America*, **116**, 24933–24942.
- Kobayashi, T. & Nishizawa, N.K. (2012) Iron uptake, translocation, and regulation in higher plants. *Annual Review of Plant Biology*, **63**, 131–152.
- Krouk, G., Lacombe, B., Bielach, A., Perrine-Walker, F., Malinska, K., Mounier, E. et al. (2010) Nitrate-regulated auxin transport by NRT1.1 defines a mechanism for nutrient sensing in plants. *Developmental Cell*, **18**, 927–937.
- Le Jean, M., Schikora, A., Mari, S., Briat, J.-F. & Curie, C. (2005) A loss-of-function mutation in *AtYSL1* reveals its role in iron and nicotianamine seed loading. *The Plant Journal*, **44**, 769–782.
- Lei, R., Li, Y., Cai, Y., Li, C., Pu, M., Lu, C. et al. (2020) bHLH121 Functions as a direct link that facilitates the activation of FIT by bHLH IVc Transcription Factors for maintaining Fe homeostasis in Arabidopsis. *Molecular Plant*, **13**, 634–649.
- Lopez, A., Cacoub, P., Macdougall, I.C. & Peyrin-Biroulet, L. (2016) Iron deficiency anaemia. *Lancet*, **387**, 907–916.
- Marqués-Bueno, M.D., Morao, A.K., Cayrel, A., Platre, M.P., Barberon, M., Caillieux, E. et al. (2016) A versatile Multisite Gateway-compatible promoter and transgenic line collection for cell type-specific functional genomics in Arabidopsis. *The Plant Journal*, **85**, 320–333.
- Martin-Barranco, A., Spielmann, J., Dubeaux, G., Vert, G. & Zelazny, E. (2020) Dynamic control of the high-affinity iron uptake complex in root epidermal cells. *Plant Physiology*, **184**, 1236.
- Mendoza-Cózatl, D.G., Xie, Q., Akmakjian, G.Z., Jobe, T.O., Patel, A., Stacey, M.G. et al. (2014) OPT3 is a component of the iron-signaling network between leaves and roots and misregulation of OPT3 leads to an over-accumulation of cadmium in seeds. *Molecular Plant*, **7**, 1455–1469.
- Palmer, C.M., Hindt, M.N., Schmidt, H., Clemens, S. & Guerinot, M. (2013) MYB10 and MYB72 are required for growth under iron-limiting conditions. *PLoS Genetics*, **9**, e1003953.
- Petit, J.-M., Briat, J.-F. & Lobréaux, S. (2001) Structure and differential expression of the four members of the Arabidopsis thaliana ferritin gene family. *The Biochemical Journal*, **359**, 575–582.
- Porra, R.J., Thompson, W.A. & Kriedemann, P.E. (1989) Determination of accurate extinction coefficients and simultaneous equations for assaying chlorophylls *a* and *b* extracted with four different solvents: verification of the concentration of chlorophyll standards by atomic absorption spectroscopy. *Biochimica et Biophysica Acta (BBA) - Bioenergetics*, **975**, 384–394.
- R Core Team (2020) *R: A language and environment for statistical computing*. R Foundation for Statistical Computing, Vienna, Austria. URL.
- Rodriguez-Celma, J., Connorton, J.M., Kruse, I., Green, R.T., Franceschetti, M., Chen, Y.-T. et al. (2019) Arabidopsis BRUTUS-LIKE E3 ligases negatively regulate iron uptake by targeting transcription factor FIT for recycling. *Proceedings of the National Academy of Sciences of the United States of America*, **116**, 17584–17591.
- Rogers, E.E., Eide, D.J. & Guerinot, M. (2000) Altered selectivity in an Arabidopsis metal transporter. *Proceedings of the National Academy of Sciences of the United States of America*, **97**, 12356–12360.
- Roschzttardtz, H., Conéjero, G., Curie, C. & Mari, S. (2009) Identification of the endodermal vacuole as the iron storage compartment in the Arabidopsis embryo. *Plant Physiology*, **151**, 1329–1338.
- Ruijter, J.M., Ramakers, C., Hoogaars, W.M.H., Karlen, Y., Bakker, O., Hoff, M.J.B. et al. (2009) Amplification efficiency: linking baseline and bias in the analysis of quantitative PCR data. *Nucleic Acids Research*, **37**, e45.
- Salomé, P.A., Bernal, M. & Krämer, U. (2014) Plant circadian networks, methods and protocols. *Methods Molecular Biology*, **1158**, 227–238.
- Schmid, N.B., Giehl, R.F.H., Döll, S., Mock, H.-P., Strehmel, N., Scheel, D. et al. (2014) FERULOYL-COA 6'-HYDROXYLASE1-dependent coumarins mediate iron acquisition from alkaline substrates in Arabidopsis. *Plant Physiology*, **164**, 160–172.
- Schneider, C.A., Rasband, W.S. & Eliceiri, K.W. (2012) NIH Image to ImageJ: 25 years of image analysis. *Nature Methods*, **9**, 671–675.
- Schulten, A., Krämer U. (2017) Interactions Between Copper Homeostasis and Metabolism in Plants. In: Cánovas F., Lüttge U., Matyssek R. (eds) *Progress in Botany* Vol. 79. Progress in Botany, vol 79. Springer, Cham. https://doi.org/10.1007/124_2017_7
- Schwarz, B. & Bauer, P. (2020) FIT, a regulatory hub for iron deficiency and stress signaling in roots, and FIT-dependent and -independent gene signatures. *Journal of Experimental Botany*, **71**, 1694–1705.
- Sgula, M., Briat, J.-F., Vert, G. & Curie, C. (2008) Cytokinins negatively regulate the root iron uptake machinery in Arabidopsis through a growth-dependent pathway. *The Plant Journal*, **55**, 289–300.
- Shin, L.-J., Lo, J.-C., Chen, G.-H., Callis, J., Fu, H. & Yeh, K.-C. (2013) IRT1 degradation factor1, a ring E3 ubiquitin ligase, regulates the degradation of IRON-REGULATED TRANSPORTER1 in Arabidopsis. *The Plant Cell*, **25**, 3039–3051.
- Sinclair, S.A., Larue, C., Bonk, L., Khan, A., Castillo-Michel, H., Stein, R.J. et al. (2017) Etiolated seedling development requires repression of photomorphogenesis by a small cell-wall-derived dark signal. *Current Biology*, **27**, 3403–3418.e7.
- Sivitz, A., Grinvalds, C., Barberon, M., Curie, C. & Vert, G. (2011) Proteasome-mediated turnover of the transcriptional activator FIT is required for plant iron-deficiency responses. *The Plant Journal*, **66**, 1044–1052.
- Sivitz, A., Hermand, V., Curie, C. & Vert, G. (2012) Arabidopsis bHLH100 and bHLH101 control iron homeostasis via a FIT-independent pathway. *PLoS One*, **7**, e44843.
- Stringlis, I.A., Yu, K.E., Feussner, K., de Jonge, R., Van Bentum, S., Van Verk, M.C. et al. (2018) MYB72-dependent coumarin exudation shapes root microbiome assembly to promote plant health. *Proceedings of the National Academy of Sciences of the United States of America*, **115**, 5213–5222.
- Thieme, C.J., Rojas-Triana, M., Stecyk, E., Schudoma, C., Zhang, W., Yang, L. et al. (2015) Endogenous Arabidopsis messenger RNAs transported to distant tissues. *Nature Plants*, **1**, 15025.
- Thomine, S., Wang, R., Ward, J.M., Crawford, N.M. & Schroeder, J.I. (2000) Cadmium and iron transport by members of a plant metal transporter family in Arabidopsis with homology to *NRAMP* genes. *Proceedings of the National Academy of Sciences of the United States of America*, **97**, 4991–4996.

- Towbin, H., Staehelin, T. & Gordon, J. (1979) Electrophoretic transfer of proteins from polyacrylamide gels to nitrocellulose sheets: procedure and some applications. *Proceedings of the National Academy of Sciences of the United States of America*, **76**, 4350–4354.
- Varotto, C., Maiwald, D., Pesaresi, P., Jahns, P., Salamini, F. & Leister, D. (2002) The metal ion transporter IRT1 is necessary for iron homeostasis and efficient photosynthesis in *Arabidopsis thaliana*. *The Plant Journal*, **31**, 589–599.
- Vert, G., Briat, J.-F. & Curie, C. (2001) Arabidopsis IRT2 encodes a root-periphery iron transporter. *The Plant Journal*, **26**, 181–189.
- Vert, G., Briat, J.-F. & Curie, C. (2003) Dual regulation of the Arabidopsis high-affinity root iron uptake system by local and long-distance signals. *Plant Physiology*, **132**, 796–804.
- Vert, G., Grotz, N., Dédaldéchamp, F., Gaymard, F., Guerinot, M.L., Briat, J.-F. *et al.* (2002) IRT1, an Arabidopsis transporter essential for iron uptake from the soil and for plant growth. *The Plant Cell*, **14**, 1223–1233.
- Wang, H.-Y., Klatte, M., Jakoby, M., Bäumlein, H., Weisshaar, B. & Bauer, P. (2007) Iron deficiency-mediated stress regulation of four subgroup Ib BHLH genes in *Arabidopsis thaliana*. *Planta*, **226**, 897–908.
- Warren, C.R. (2008) Rapid measurement of chlorophylls with a microplate reader. *Journal of Plant Nutrition*, **31**, 1321–1332.
- Waters, B.M., McInturf, S.A. & Stein, R.J. (2012) Rosette iron deficiency transcript and microRNA profiling reveals links between copper and iron homeostasis in *Arabidopsis thaliana*. *Journal of Experimental Botany*, **63**, 5903–5918.
- Winter, D., Vinegar, B., Nahal, H., Ammar, R., Wilson, G.V. & Provart, N.J. (2007) An “Electronic Fluorescent Pictograph” browser for exploring and analyzing large-scale biological data sets. *PLoS One*, **2**, e718.
- Wintz, H., Fox, T., Wu, Y.-Y., Feng, V., Chen, W., Chang, H.-S. *et al.* (2003) Expression profiles of *Arabidopsis thaliana* in mineral deficiencies reveal novel transporters involved in metal homeostasis. *Journal of Biological Chemistry*, **278**, 47644–47653.
- Yang, T., Lin, W.-D. & Schmidt, W. (2010) Transcriptional profiling of the Arabidopsis iron deficiency response reveals conserved transition metal homeostasis networks. *Plant Physiology*, **152**, 2130–2141.
- Zamioudis, C., Hanson, J. & Pieterse, C.M. (2014) β -Glucosidase BGLU42 is a MYB72-dependent key regulator of rhizobacteria-induced systemic resistance and modulates iron deficiency responses in Arabidopsis roots. *New Phytologist*, **204**, 368–379.
- Zamioudis, C., Korteland, J., Pelt, J.A.V., Hamersveld, M., van Dombrowski N., Bai Y. *et al.* (2015) Rhizobacterial volatiles and photosynthesis-related signals coordinate MYB72 expression in Arabidopsis roots during onset of induced systemic resistance and iron-deficiency responses. *The Plant Journal*, **84**, 309–322.
- Zheng, L., Baumann, U. & Reymond, J.L. (2004) An efficient one-step site-directed and site-saturation mutagenesis protocol. *Nucleic Acids Research*, **32**, e115.
- Zuo, Y. & Zhang, F. (2011) Soil and crop management strategies to prevent iron deficiency in crops. *Plant and Soil*, **339**, 83–95.